Surface Eddy Momentum Flux and Velocity Variances in the Southern Ocean from Geosat Altimetry

ROSEMARY MORROW,* RICHARD COLEMAN,†,**,†† JOHN CHURCH,**,†† AND DUDLEY CHELTON@

*GRGS/CNES, Toulouse, France
†Department of Surveying and Spatial Information Science, University of Tasmania, Tasmania, Australia
**C.R.C. for the Antarctic and Southern Ocean Environment, University of Tasmania, Tasmania, Australia
††CSIRO, Division of Oceanography, Hobart, Tasmania, Australia
@College of Oceanic and Atmospheric Sciences, Oregon State University, Corvallis, Oregon

(Manuscript received 20 April 1993, in final form 7 January 1994)

ABSTRACT

Satellite altimetry has previously been used to map the magnitude of the surface eddy variability of the global oceans, but the direction of the time-variable velocities have been more difficult to determine. Here, a technique is presented for resolving both magnitude and direction of residual surface geostrophic velocities at Geosat altimeter crossover points; providing a two-year time series with a temporal resolution of 17 days and horizontal resolution of around 100 km. The time series of residual velocity components are then used to determine surface eddy statistics in the Southern Ocean and to investigate the role of transient eddies in the Southern Ocean momentum balance. The surface eddy statistics from Geosat crossover points show a complex spatial distribution in the surface Reynolds stresses ($\overline{u'^2}$, $\overline{v'^2}$, $\overline{u'v'}$). In contrast to the assumptions of isotropic variability in previous analyses of altimeter data, velocity variance ellipses are found to be distinctly anisotropic in many regions. The surface eddy statistics compare favorably with the available in situ current meter data and surface drifter data. The complex spatial distribution of surface eddy momentum flux is strongly influenced by bottom topography and the position of the mean current. On a zonal average, the horizontal divergence of eddy momentum flux from transient eddies is found to be around two orders of magnitude too small to directly balance the eastward momentum from the wind. In the Agulhas Return Current and near the Macquarie Ridge/Campbell Plateau, the Reynolds stresses are significant and they act to concentrate the mean jet, in agreement with recent numerical models. However, circumpolar streamwise averages along paths parallel to the mean axis of the Antarctic Circumpolar Current show only a small net convergence.

1. Introduction

The Southern Ocean is unique in being the only zonally unbounded oceanic region, and provides a major link by which water properties are exchanged among the Atlantic, Indian, and Pacific Oceans. It is a region of large heat and momentum exchanges between the ocean and the atmosphere. The large 3×10^{14} W heat loss south of the Antarctic Circumpolar Current (ACC) (Gordon and Taylor 1975) implies a southward oceanic heat flux of the same magnitude across the circumpolar band (Gordon 1981), which may be accomplished by eddy heat fluxes (de Szoeke and Levine 1981; Bryden 1979). Ocean eddies may also play an important role in transporting momentum in the circumpolar region (Gill 1968; McWilliams et al. 1978; Wolff et al. 1991).

The role of eddies in the Southern Ocean momentum balance has been the subject of numerous theories and numerical models over the last four decades. Strong westerly winds input a large amount of momentum into the Southern Ocean, but the absence of any continental boundaries between 56° and 61°S means that Sverdrup balance cannot apply at these latitudes. The wind input of momentum cannot be balanced by horizontal or vertical diffusion alone (assuming the normal range of diffusion parameters), as the resulting model transports through Drake Passage are much greater than observed (Gill 1968; McWilliams et al. 1978). Gill (1968) suggested that eddies may act to transport eastward momentum meridionally away from the axis of the ACC. Another theory is that topographic form stress may balance the momentum input by the wind. This form stress can be set up as the mean current flows over bottom topography (Munk and Palmén 1951) or as eddies interact with topography (Holloway 1987).

Recent models (Johnson and Bryden 1989; Treguier and McWilliams 1990; Wolff et al. 1991) suggest that transient and standing eddies may provide the mechanism for transferring the zonal momentum vertically downward to be removed by bottom topographic form stress. Marshall et al. (1993) note that standing eddies are an artifact of choosing a zonal–meridional coor-

Corresponding author address: Dr. Rosemary Morrow, GRGS/CNES, 18 Avenue Edouard Belin, Toulouse, 31055 France.

dinate system, and cannot play a role in the actual momentum balance for the ACC. In these models, the horizontal eddy momentum fluxes from transient eddies act to concentrate and strengthen the mean flow, rather than transport momentum away from the circumpolar band as suggested by Gill (1968).

Ideally, these theories and models should be tested against global observations at all depth levels. Unfortunately, there are limited long-term observations of eddies in the Southern Ocean to differentiate between these theories. The main problem in measuring eddy variability is that the eddies occur everywhere in the ocean over a wide range of space and time scales. To adequately measure the meandering currents and eddies requires high horizontal resolution ($\sim$10 km) and short time resolution ($\sim$10 days); high vertical resolution is not necessary as only a small number of modes are required to represent the vertical structure in the ocean (Hurlburt 1986). In the Southern Ocean, the problem of measuring eddies is compounded by the difficulty and expense of maintaining the traditional current meter moorings in this remote region.

The regular repeat sampling of satellite altimeter data has the potential for providing long term global observations of surface eddy statistics, especially at middle to high latitudes (Fu and Zlotnicki 1989). Previous satellite altimeter studies have confirmed the presence of a vigorous eddy field in the Southern Ocean, with large geographical variations (Cheney et al. 1983; Zlotnicki et al. 1989). Regions of high eddy energy are shown to be strongly controlled by the position of the mean flow and bottom topography (Sandwell and Zhang 1989; Chelton et al. 1990). This is supported by theoretical studies that show the interaction of a zonal current with topography is important in the generation of instabilities and eddies (e.g., McCartney 1976; Thompson 1993).

Observations of the vertical and horizontal eddy momentum fluxes are limited in the Southern Ocean. The vertical eddy momentum flux has not been measured directly, but the downward transfer of zonal momentum by eddy form drag has been estimated at Drake Passage from the meridional eddy heat flux and the vertical temperature gradient (Johnson and Bryden 1989). Horizontal eddy momentum fluxes have only been observed at a few current meter locations in the Southern Ocean (e.g., Wright 1981; Bryden and Heath 1985; Luyten et al. 1990). These results give differing estimates of the magnitude of the horizontal eddy momentum flux. To examine the eddy contribution to the zonal momentum balance, Bryden and Heath (1985) extrapolated these "point source" results around the entire circumpolar region and found that horizontal eddy momentum fluxes could account for only 25% of the momentum input by the wind. Given the large spatial variations in the eddy field, is this extrapolation correct?

The zonally averaged surface momentum flux has been estimated from the FGGE surface drifter measurements (Piola et al. 1987). The results show a momentum flux out of the region of order 60 $cm^2\ s^{-2}$, with the main contribution from the mean flow and standing eddies. The zonally averaged eddy momentum flux from transient eddies is smaller, around 5 $cm^2\ s^{-2}$, except for a large positive flux of 27 $cm^2\ s^{-2}$ at 51°S. There are large errors associated with these calculations (Piola 1987), which are attributed to the irregular temporal and spatial sampling of the data. Moreover, the drifter results may be biased toward higher energy frontal regions (Hofmann 1985).

The distribution of anisotropic eddy kinetic energy and horizontal eddy momentum flux has been difficult to determine from surface altimeter data. This is due to the problem of resolving north/east directional components of the surface velocities from the alongtrack altimeter data. The traditional approach in altimetric studies is to resolve the across-track component of geostrophic velocity from the alongtrack sea surface slope, then assume the flow is isotropic to estimate the eddy kinetic energy. The assumption of isotropic variability may not be valid, especially in regions of strong currents or close to topography. The two components of the surface residual velocity vector have been resolved from mapped altimeter sea surface height data (Tai and White 1990; Chelton et al. 1990), although the objective mapping filters out most of the variance associated with smaller-scale eddies.

In this paper, an alternate technique is presented that resolves the magnitude and direction of residual surface geostrophic velocities at Geosat crossover points into conventional (u, v) components, while maintaining a spatial resolution of about 100 km, set by the satellite measurement noise and pattern. This method is used to obtain a *time series* of orthogonal surface velocity components at each altimeter crossover point, from which we resolve directional eddy variability statistics and determine the geographic distribution and the anisotropic structure of the surface mesoscale variability. The technique also allows a direct measurement of the surface eddy momentum flux over the Southern Ocean, as described by Morrow et al. (1992). A similar method was applied by Johnson et al. to examine Reynolds stresses in the southeast Pacific Ocean. The results over the entire Southern Ocean permit an investigation of the role of transient eddies in the zonal momentum balance of the ACC, especially in the high eddy energy regions where the ACC interacts with bottom topography.

The paper proceeds with a description of the Geosat data and the processing techniques that are required to extract residual sea surface height data from the altimeter measurements (section 2). The method for resolving orthogonal velocity components at altimeter crossover points is discussed in section 3 (a detailed error analysis for the Geosat measurements is presented

in the appendices). The velocity variance from (u', v') components is presented in the form of variance ellipses in section 4, which show the magnitude and the principal direction of the variance. The altimeter velocity variance statistics are compared with independent velocity measurements from surface drifters and in situ current meter records. In section 5, the distribution of the surface eddy momentum flux field (or horizontal Reynolds stress) is presented for the Southern Ocean. The zonally averaged eddy momentum flux is discussed in relation to the zonal momentum balance. To investigate the transfer of momentum between eddies and the mean current, "streamwise" averages of the Reynolds stress components are calculated, relative to a mean current determined from independent hydrographic data. Section 6 sets out a discussion of the results and conclusions of the study.

2. Geosat data processing

The following calculations are based on two years of Geosat radar altimeter data, from the start of the 17-day Exact Repeat Mission commencing in November 1986. The Geosat satellite orbit gives a longitudinal spacing between ground tracks of around 150 km at the equator, converging to around 75 km at 60°S. A full description of the techniques used to measure sea surface height from altimetry and the associated errors is given in Chelton (1988). For a description of the Geosat mission see Douglas and Cheney (1990).

The Geosat data used in this study are based on the Zlotnicki/Fu dataset from the NASA Ocean Data System at the Jet Propulsion Laboratory (Zlotnicki et al. 1989, 1990). The data are corrected for the standard atmospheric and geophysical errors as described in Cheney et al. (1987), including corrections for wet and dry troposphere range delays, ionospheric range delays, solid earth and ocean tides, and the inverse barometer effect on sea level by atmospheric pressure loading. The sea state bias is corrected using the Witter and Chelton (1991) algorithm. Satellite orbits were based on the GEM-T2 orbit model (Haines et al. 1990). The corrected height data were edited to remove anomalous points, all flagged data, and measurements over land following the procedures of Zlotnicki et al. (1990). This includes rejecting data records with sigma height values greater than 10 cm; attitude angles greater than 1 degree and automatic gain control less than 16 dB or greater than 40 dB. The height data were then interpolated using a cubic spline routine to a fixed geographical grid at approximately 7-km spacing, corresponding to the uniform latitudinal grid of Zlotnicki et al. (1990). This process simplifies the removal of the geoid and orbit errors from each pass and is computationally more efficient.

Residual orbit errors were removed from the global dataset for the two-year period November 1986 to November 1988 (ERMs 1-43) by Chelton and Schlax (1993), using an extension of the method developed by van Gysen et al. (1992). Sea surface height residuals were extracted for our Southern Ocean study area, from longitudes 0°–360°E and latitudes 30°–60°S (limited to the south by sea ice contamination).

3. Resolving orthogonal velocity components at crossover points

Residual sea surface velocities can be calculated from the smoothed alongtrack sea surface slope using the geostrophic relation; that is, for an ascending pass,

$$V_{a'} = \frac{g}{f}\frac{dh}{dx}, \tag{3.1}$$

where g is gravitational acceleration, f is the Coriolis parameter, x is the alongtrack direction, and h is the residual sea surface height (SSH) after the removal of the mean and orbit errors, as described in section 2. The sea surface slope is calculated by fitting a 25-point linear regression to the alongtrack residual heights. The transfer function of this filter has a reasonably sharp cutoff in the wavenumber domain, which preserves most of the variability at wavelengths greater than 100 km (Schlax and Chelton 1992). This filtering was necessary because of the 3–5 cm rms measurement noise in the Geosat data. Any eddy variability at shorter space scales will be indistinguishable from the measurement noise, and thus cannot be resolved by Geosat data (Fu and Zlotnicki 1989). It should be noted that typical eddies at high southern latitudes have spatial correlation scales of 30–40 km (corresponding to a radius of deformation of 10 km) and integral timescales of 14–16 days (Bryden and Heath 1985). The smoothed height data analyzed here cannot resolve the shortest eddy scales and therefore may miss a significant fraction of the eddy energy. However, the resolution and sampling density of the Geosat data are better than those of all previous datasets, such as drifters or current meters.

The direction of the eddy velocities cannot be determined from this calculation since we are measuring only the cross-track component of the residual flow. The Geosat orbit configuration produces ground tracks that are aligned at 21° from north at the equator, and around 45° from north at 65°S (Parke et al. 1987). Thus, the traditional maps of EKE derived from cross-track velocities and assuming isotropic variability have an intrinsic bias—they measure more zonal variability near the equator and equal parts of zonal and meridional flow at 65°S. As we will see, the eddy variability we are measuring can be distinctly anisotropic, especially in regions of strong mean currents (Richardson 1983) or in the vicinity of bottom topographic features. Resolving orthogonal components of eddy variability is also necessary for calculating the horizontal eddy momentum flux.

The magnitude and direction of the residual velocity can be resolved at crossover points by a simple geometric transformation. Here, we have available two (generally nonorthogonal) components of geostrophic velocity from each of the ascending and descending passes ($V_{a'}$, $V_{d'}$), and a known angle (ϕ) between the ground track and the north meridian, which varies as a function of latitude only. The residual velocity can be calculated in any orthogonal projection, for example, in east/north components (u', v') following Parke et al. (1987):

$$u' = \frac{V_{a'} + V_{d'}}{2\cos\phi} \tag{3.2}$$

$$v' = \frac{V_{a'} - V_{d'}}{2\sin\phi}. \tag{3.3}$$

The errors associated with the geometric transformation in Eqs. (3.2) and (3.3) can also be determined. If the residual sea surface slope measurements from the ascending and descending passes have a variance error of $\sigma_{s'}^2$, then using the law of propagation of variances and assuming $V_{a'}$ and $V_{d'}$ are independent, the variance of the errors in the u' and v' components will be

$$\sigma_{u'}^2 = \frac{1}{2}\left(\frac{g\sigma_{s'}}{f\cos\phi}\right)^2 \tag{3.4}$$

$$\sigma_{v'}^2 = \frac{1}{2}\left(\frac{g\sigma_{s'}}{f\sin\phi}\right)^2. \tag{3.5}$$

If there were no measurement errors in the corrected altimeter data, the geometrical transformation of Eqs. (3.2) and (3.3) would resolve the orthogonal velocities perfectly. However, Eqs. (3.4) and (3.5) show that the error in each velocity component depends on the estimated measurement error $\sigma_{s'}$, that is, how well the geostrophic sea surface slopes can be estimated from the filtered alongtrack residuals. The error in u' and v' will also vary with latitude, depending on three factors: the Coriolis parameter f, the crossover angle ϕ, and the time difference between the ascending and the descending passes. For a detailed discussion of these errors, especially in regard to the Geosat mission, the reader is referred to the appendix.

4. Velocity variance in the Southern Ocean

Velocity variance statistics were calculated from the two-year time series of 8.5-day interpolated u', v' velocity components, at each crossover point. From this time series we can compute the north/east velocity variance terms ($\overline{u'^2}$, $\overline{v'^2}$) and the covariance term $\overline{u'v'}$. The magnitude and the direction of the eddy variability are represented here using variance ellipses (see Preisendorfer 1988). The direction, θ, of the axis of principal variability, measured anticlockwise from east, is

$$\tan\theta = \frac{\sigma_{11} - \overline{u'^2}}{\overline{u'v'}}, \tag{3.6}$$

where σ_{11} is the variance along the major axis and is given by

$$\sigma_{11} = \frac{1}{2}\left(\overline{u'^2} + \overline{v'^2} + \sqrt{(\overline{u'^2} - \overline{v'^2})^2 + 4(\overline{u'v'})^2}\right) \tag{3.7}$$

and along the minor axis by

$$\sigma_{22} = (\overline{u'^2} + \overline{v'^2}) - \sigma_{11}. \tag{3.8}$$

Anisotropic flow is represented by an elongated ellipse, with the principal direction of the velocity variance aligned with the direction of the major axis. The orientation of the ellipse depends on the covariance term, $\overline{u'v'}$; the major and minor ellipse axes define the coordinate system in which u' and v' are uncorrelated. Ellipses with a major axis oriented in the northeast quadrant have a positive $\overline{u'v'}$; ellipses oriented toward the southeast quadrant have a negative $\overline{u'v'}$. Thus the direction of eddy momentum flux can be inferred simply from the ellipse orientation.

a. Velocity variance ellipses on a 5° grid

Velocity variance ellipses reveal the principal direction and anisotropic nature of the variability, as well as the magnitude and spatial distribution of the eddy energy. The velocity variance ellipses for the Southern Ocean, calculated from ensemble-averaged statistics on a 5° grid, are shown in Fig. 1. The 5° grid spacing was chosen at the same resolution as most of the FGGE drifter studies (e.g., Patterson 1985; Daniault and Menard 1985). The magnitude of the two datasets are comparable in the boundary current regions of the Agulhas Retroflection, the east Australian Current, and the southwest Atlantic. The main differences occur in the ACC, where the 5° binned FGGE drifter measurements can be up to ten times larger than the Geosat results. Because the drifters tend to converge toward the narrow, highly energetic frontal zones (Hofmann 1985), the drifter velocities are biased toward the small fraction of the 5° bin that has a higher EKE. The more regularly spaced Geosat measurements sample high and low energy regions equally, and thus provide more accurate 5° averages in frontal regions.

The Geosat ellipses show little eddy activity over topographic ridges and shallow plateaus, while the higher eddy energy occurs in the deep basins, adjacent to major topographic features. These results are consistent with recent numerical models (Treguier and McWilliams 1990; Wolff et al. 1991) and earlier altimetric studies based on sea surface height variability (Sandwell and Zhang 1989; Chelton et al. 1990). The variance ellipses appear isotropic along the axis of the ACC. Distinct anisotropic variability is most evident

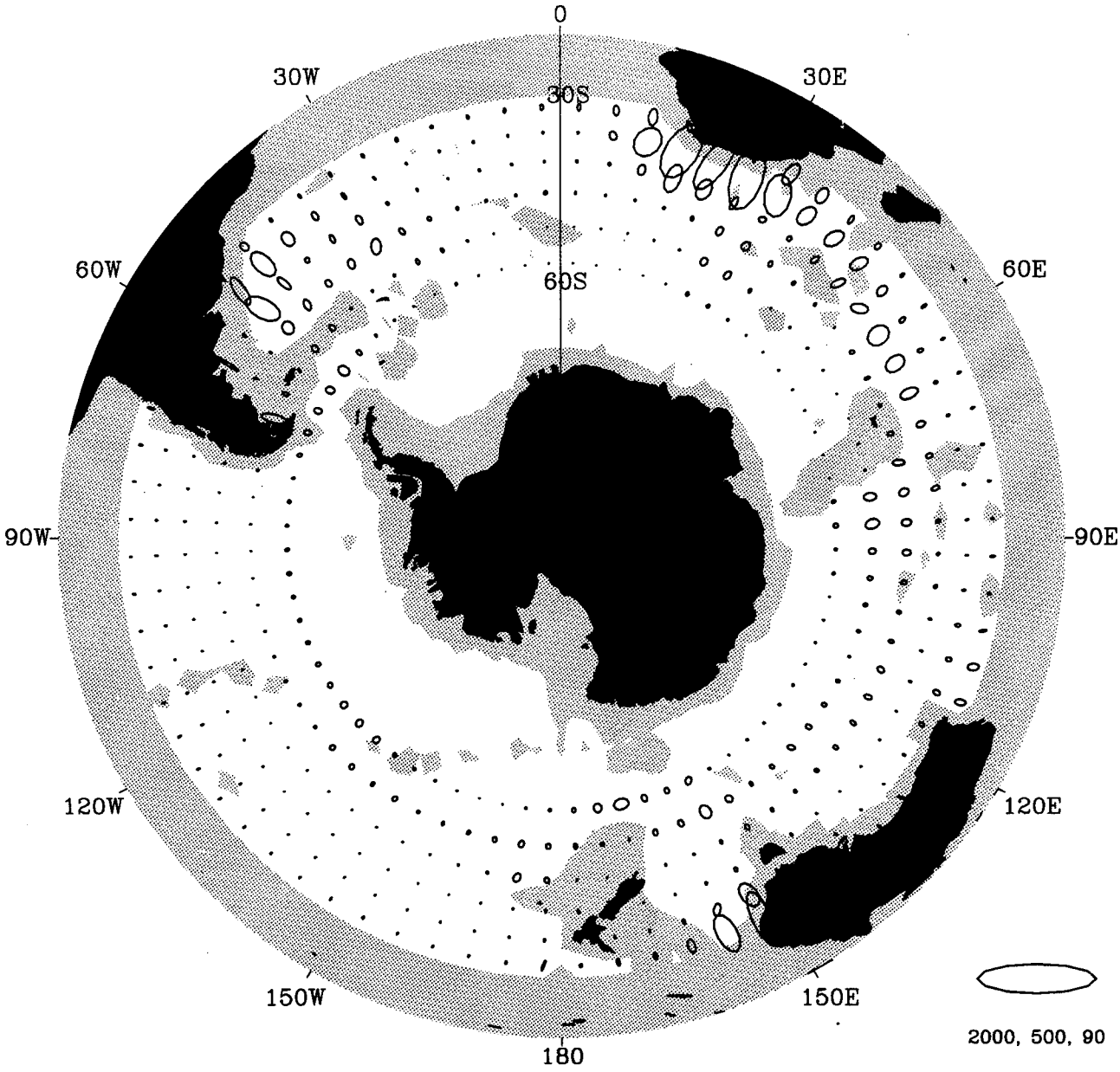

FIG. 1. Velocity variance ellipses for the Southern Ocean from Geosat crossover velocities ensemble averaged on a 5° grid. The position of the 3000-m depth contour is shaded gray. The scale ellipse has a semimajor axis of 2000 $cm^2 s^2$, a semiminor axis of 500 $cm^2 s^2$, and is rotated by 90° from north.

in the high eddy energy regions of the Agulhas Retroflection and Return Current, the East Australian Current and the southwest Atlantic region, and is probably influenced by meridional shifts in the zonal jet. Anisotropic ellipses are also noted where the mean current interacts with bottom topography, for example, across the Madagascar Ridge at 40°E and the Macquarie Ridge at 170°E. Ellipses on a smaller 3° grid reveal more of the anisotropic nature of the variability (Morrow et al. 1992).

b. Velocity variance ellipses at individual crossover points

An advantage of the present technique is the ability to resolve variations in the EKE distribution on scales

of order 100 km over the entire ocean basin. Maintaining the fine spatial resolution is especially important in the Southern Ocean, where abrupt changes in topography cause a similar response in the eddy field.

Velocity variance ellipses are derived from the individual Geosat crossover points in the Agulhas Retroflection and Return Current (Fig. 2), southeast of Australia (Fig. 3), and in the southwest Atlantic region (Fig. 4). At this resolution the anisotropy of the eddy variance is apparent. Close to coastlines and near major topographic features, there is a strong tendency for variance ellipses to align with the bottom topography (see in particular Fig. 3). The ellipses immediately adjacent to the east of Australia are oriented parallel to the east Australian coast, and there is distinct steering of the ellipse angles around the Campbell Plateau at 55°S,170°E. Similarly, in the southwest Atlantic region (Fig. 4), the higher variability is bounded by shallower topography, and along the boundaries the ellipses tend to align with the bathymetry.

In regions of higher variability away from topographic features, the ellipses are also anisotropic. This is noted in regions where the mean current is strong and narrow, or meanders, for example, in the Agulhas Retroflection and Return Current, in the East Australian Current, and downstream of the Macquarie Ridge and Drake Passage. There are sharp spatial gradients in the magnitude and direction of the ellipse variability between adjacent crossover points. This particularly occurs across the axis of the mean current, and between regions of high and low eddy energy. These distinct spatial gradients reaffirm the need to maintain the highest spatial resolution possible. Along the path of the mean current, the ellipse magnitude and orientation tend to be more coherent between neighboring crossover points. This suggests that the processing tech-

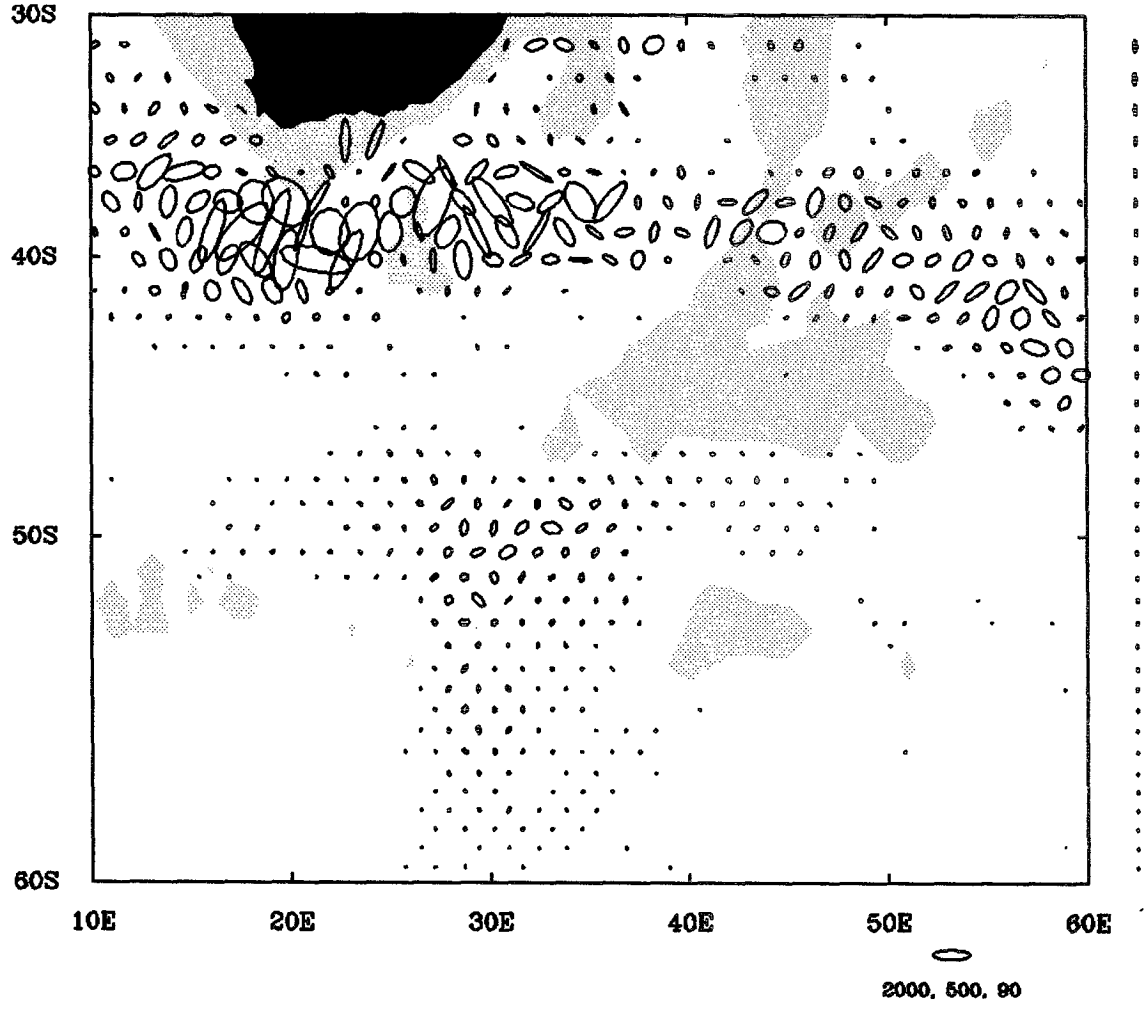

FIG. 2. Velocity variance ellipses for the Agulhas Retroflection region from the time series of velocity components at Geosat crossover points. Only variance ellipses above the estimated background noise level are shown. Estimated background noise ellipses are constant at each latitude (see text), shown on the right-hand side of the plot. The position of the 3000-m depth contour is shaded gray. The scale ellipse is described in Fig. 1.

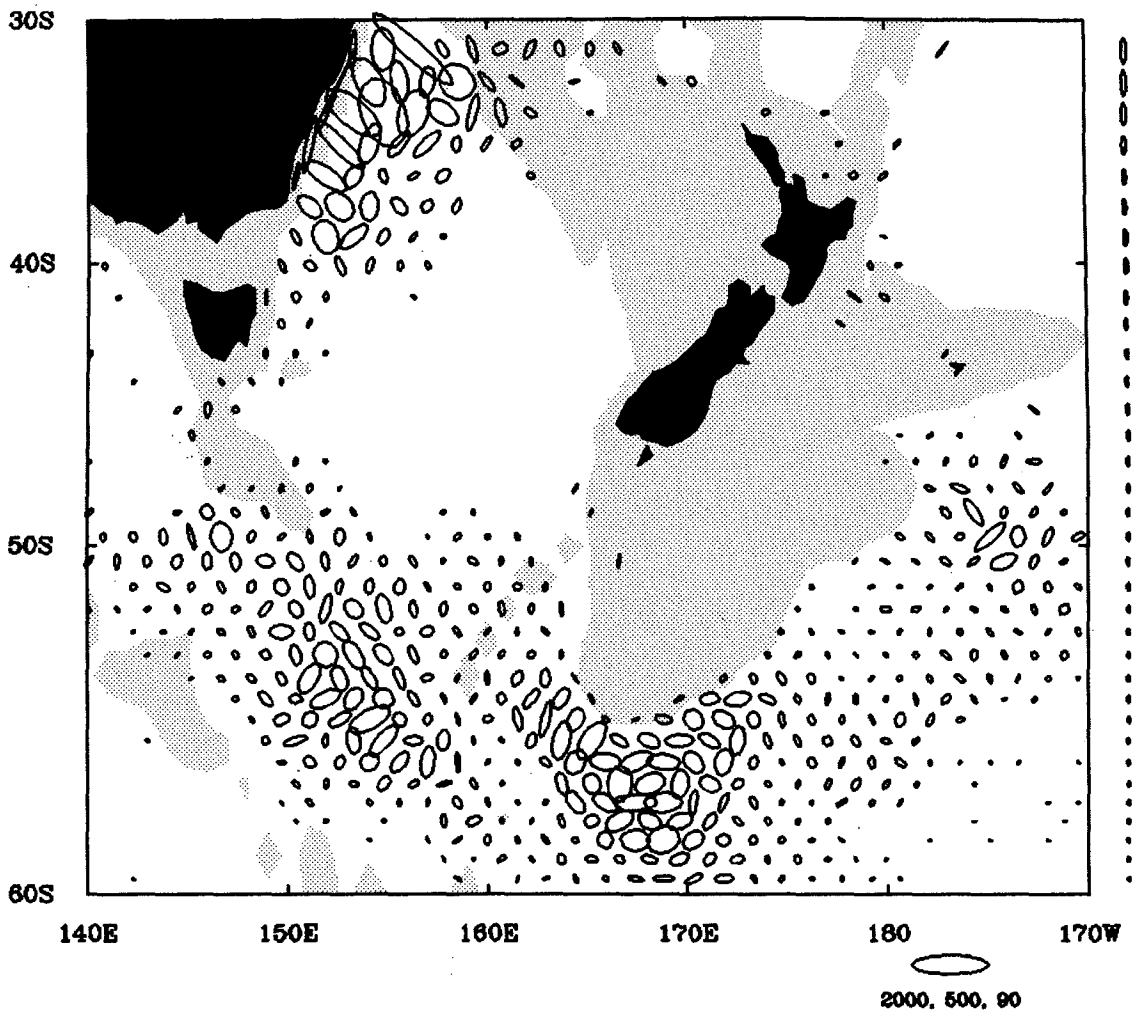

FIG. 3. As in Fig. 2 but for the region southeast of Australia and New Zealand.

niques for interpolating and smoothing the velocity data are preserving coherent oceanographic signals.

Recent numerical models have found that the eddy variability tends to be anisotropic in the region of strong mean currents. In a flat-bottom quasigeostrophic model of the Southern Ocean circulation, Wolff et al. (1991) found that eddy ellipses northward of the current were tilted from northwest to southeast, whereas eddies south of the current were tilted from southwest to northeast. This structure is also apparent in the Geosat data, for example, upstream of Kerguelen Plateau at 50°E and upstream of the Macquarie Ridge at 160°E. In these cases, the eddy momentum flux tends to be directed so as to transport zonal momentum toward the central jet. The tilted ellipses may be caused by the reduction of the intrinsic Rossby wave phase speed by the central current (McWilliams and Chow 1981).

Similar patterns are also evident in variance ellipses derived from 30 years of fine-resolution surface drifter data in the East Australian Current region (Morrow et al. 1992) and from an eddy-resolving numerical model (Wilkin and Morrow 1994). The altimeter variance ellipses tend to be less isotropic than the 1° binned drifter data and show sharper spatial gradients between regions of high and low energy. The bulk variance statistics are similar (Morrow et al. 1992), although there are regional differences in magnitude. For example, in the high eddy energy region (30°–40°S, 150°–160°E), the altimeter variance of 602 $cm^2\ s^{-2}$ is greater than the drifter variance of 456 $cm^2\ s^{-2}$; whereas in the low energy region (30°–40°S, 170°–180°E), the drifter variance of 113 $cm^2\ s^{-2}$ is larger than the Geosat variance of 96 $cm^2\ s^{-2}$, which is at the background noise level. Besides the different spatial and temporal sampling of the datasets, it is not known how faithfully the drifters follow the surface currents, since the buoys are subject to windage. Drifter data also include an unknown ageostrophic component (Large and van Loon 1989) and therefore may not be directly compatible with the altimeter data.

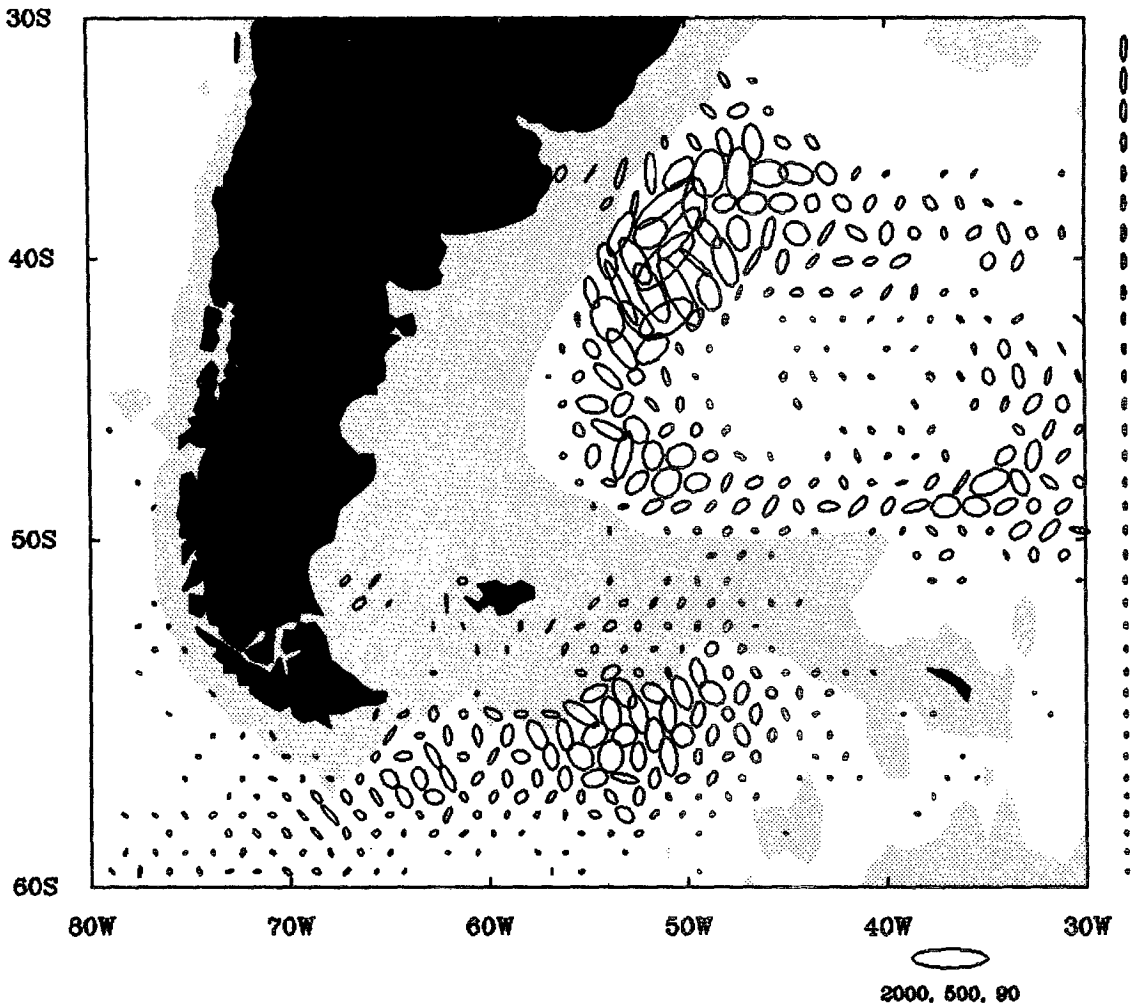

FIG. 4. As in Fig. 2 but for the southwest Atlantic region.

This analysis only considers Geosat velocity variance ellipses greater than the estimated background noise variance. Background error ellipses are calculated by using Eq. (A.2) as an estimate of the background SSH error, then propagating that estimate through Eqs. (3.4) and (3.5), and then (3.6), (3.7), and (3.8). These background error ellipses are constant along crossover latitude lines (see appendix B), and represent the error dependence on the Coriolis parameter, the crossover angle, and the crossover time difference. Error ellipses are plotted on the right-hand side of Figs. 2, 3, and 4, assuming the errors in the two velocity components are uncorrelated. An increase in the northward component of error variance is apparent toward the equator, especially between 20°S and 30°S. As discussed in the appendices, these errors are intrinsic to the orbit configuration of each altimeter mission and limit the analysis to higher latitudes. In this paper, the analysis is restricted to the region south of 30°S. Highly energetic regions within 30° of the equator may still be analyzed where the signal-to-noise ratio is sufficiently large.

Ellipses with large variance that exceed the background noise level may still not be statistically significant. The statistical significance of the variance is calculated based on the number of degrees of freedom (ndf), which is approximately equal to the number of data points at each crossover point (see appendix B). Based on the ndf, a statistical F-test table (Table A.1) is used to estimate how close we are to the expected variance of an infinite number of samples. On average we have 30 degrees of freedom at each crossover point, so we are within 50% of the expected variance for an infinite time series. Even with our maximum ndf at each crossover point of 43 (assuming no data gaps), we are only within 40% of the expected variance. Any improvement in the statistical significance requires a much longer time series, or some spatial averaging (as in section 4a) at the expense of the 100-km spatial resolution.

c. Comparison with in situ current meter data

The Geosat velocity variance ellipses measure temporal variability at a fixed location (the crossover point). This is analogous to making surface velocity measurements from a current meter mooring; albeit current meters have a faster sampling rate, measure both the geostrophic and ageostrophic motion, and measure both velocity components concurrently and without the spatial filtering over 100 km.

Nevertheless, it is constructive to compare the Geosat velocity variance with statistics from long-term current meter arrays. The surface EKE from Geosat data were bilinearly interpolated from the four closest crossover points onto mooring locations, in the Agulhas Retroflection (Luyten et al. 1990) and southeast of New Zealand (Bryden and Heath 1985) (see Table A.1 in Morrow et al. 1992). Geosat variances were in general a factor of 1.5 to 2 times greater than the current variability at the shallowest depths (200 m in the Agulhas and 1000 m southeast of New Zealand). Vertical profiles of the composite statistics (Morrow 1992) show that the surface intensification is consistent with the strong current shear observed at the deeper records.

A 3-month overlap between the Agulhas deployment times and the start of the Geosat mission also allows a direct time series comparison between the two datasets. Figure 5 shows the velocity time series from the Agulhas current record 838 at a median depth of 205 m, compared to the surface velocity time series from the closest Geosat crossover point (32 km northwest of the current meter location). This current meter time series was chosen as an example as it has the longest overlapping period with the Geosat mission. The north and east velocity components and the stick velocity vectors from the two datasets show good agreement, although the in situ current meter records show more high-frequency signal than can be resolved by the surface altimeter velocities, interpolated to 8.5 days. Considering the different limitations of the current meter and altimeter datasets, the comparison in Fig. 5 is very encouraging.

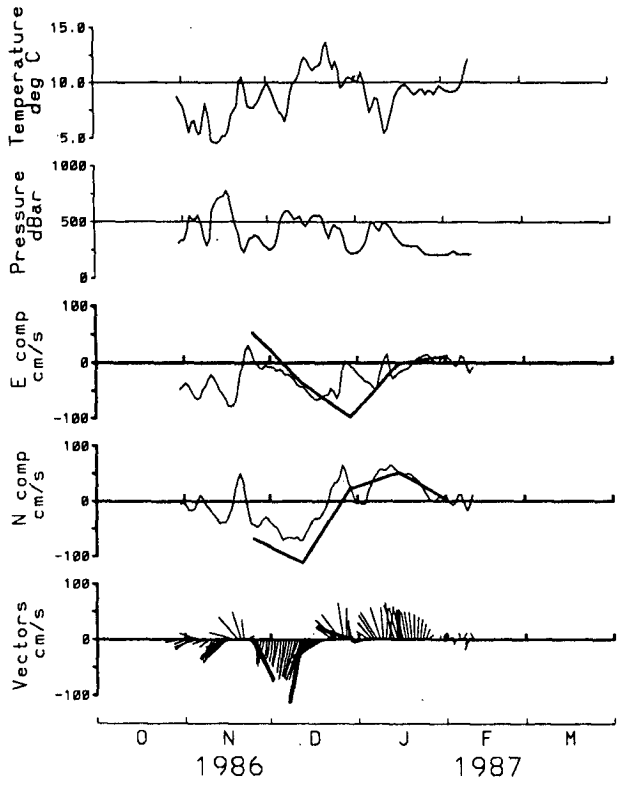

FIG. 5. Time series of current meter data in the Agulhas Retroflection at 38°S,18.5°E from the shallowest meter at 195 m from Luyten et al. (1990) for the three months from November 1986. The heavy line denotes the Geosat surface velocities in north/east coordinates from the closest crossover point, 32 km to the northwest, measured over the same time period.

5. Distribution of eddy momentum flux

The distribution of surface horizontal eddy momentum flux gives us some insight into the dynamical processes of the ACC. In particular, the mapped distribution can show whether eddies act to transport momentum away from the region of wind forcing, or into or away from the mean current. The geographical distribution also suggests the importance of bottom topography in this interaction.

To first order, the ACC can be considered a zonal current. In this case, the cross-stream flux of alongstream momentum by transient eddies is given by $\overline{u'v'}$. The interaction of the mean current with bottom topography produces a complex pattern of $\overline{u'v'}$ in the Southern Ocean. To investigate the larger-scale patterns of $\overline{u'v'}$, the data were ensemble averaged on a 2° latitude by 5° longitude grid (Fig. 6). This grid was chosen to increase the statistical reliability of the variance and covariance estimates and because we expect larger coherence in the alongstream direction, as discussed previously. In the Agulhas Return Current from 20° to 80°E, there is a general pattern of eddy momentum flux convergence with positive $\overline{u'v'}$ to the south (dark in Fig. 6) and negative $\overline{u'v'}$ to the north (light) of the eastward mean current. Convergence of eddy momentum flux is also noted upstream and downstream of the Macquarie Ridge near 150°E, and near the Pacific Mid-Ocean Ridge at 140°W. There are also limited regions of eddy momentum flux divergence, for example, downstream of the Pacific Mid-Ocean Ridge at 110°W.

The altimeter observations in Fig. 6 are more complex than a simple convergence of $\overline{u'v'}$ along the mean axis of a zonal current. When there is a northward (southward) deflection of the mean current (i.e., a time-independent meander), there is a corresponding northward (southward) horizontal momentum flux from transient eddies and meanders. In the Agulhas

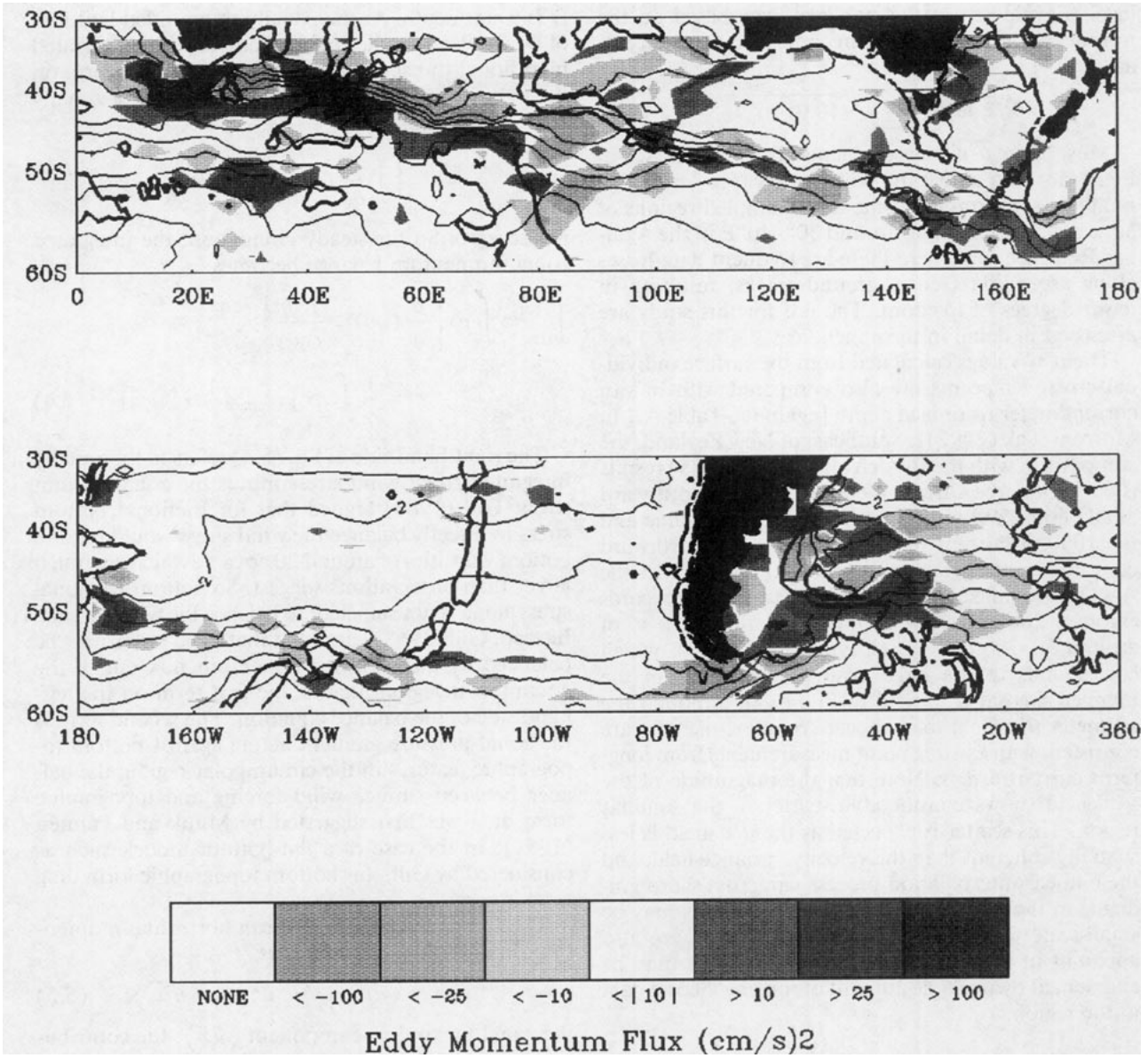

FIG. 6. Eddy momentum flux $\overline{u'v'}$ from Geosat crossover velocities, composite averaged onto a 2° latitude by 5° longitude grid. The thick black lines denote the 3000-m depth contour. The thin black lines show the 0/2000 dbar dynamic topography with a contour interval of 20 cm from Gordon and Monelli (1982).

Return Current, as the mean current is forced north of the Del Cano Rise at 45°E, there is a northward flux of eastward momentum over a wide range of latitudes. In the Crozet Basin downstream, the mean current deflects back to the south and there is a southward flux of eastward transient eddy momentum across the mean current. This pattern is repeated downstream of Kerguelen Plateau at 90°E. In the southwest Atlantic region, the complex pattern of positive and negative $\overline{u'v'}$ is reflected by the strong topographic gradients. It appears that the horizontal transient eddy momentum flux may have a role in steering the mean current around bottom topography and in changing its position.

To test whether these eddy momentum flux calculations are significantly different from zero, the cross-correlation coefficient $C_{u'v'}$ is calculated at each crossover point, following Bryden (1979):

$$C_{u'v'} = \frac{\overline{u'v'}}{\sqrt{(u'^2v'^2)}}. \qquad (5.1)$$

The cross-correlation coefficient is then compared with the 95% significance level to test the statistical significance of the $\overline{u'v'}$ calculations. The 95% significance

level is evaluated in the standard way, based on the number of degrees of freedom (ndf) (see appendices), as

$$95\%\ \text{level} = \sqrt{1 - (0.05)^{(\text{ndf})^{-1}}}. \qquad (5.2)$$

Most of the $\overline{u'v'}$ measurements above 25 cm^2 s^{-2} in Fig. 6 are also above the 95% significance level. The notable exceptions are some undersampled regions of large $\overline{u'v'}$, for example, around 30°–40°E in the Agulhas Retroflection where there are frequent data losses along ascending Geosat ground tracks, resulting in fewer degrees of freedom. The ndf for this study are discussed in detail in the appendices.

The $\overline{u'v'}$ values calculated from the surface individual crossover points are also compared with in situ current meter records at depth [again see Table A.1 in Morrow et al. (1992)]. Southeast of New Zealand, the comparison with the Bryden and Heath (1985) results is very good; the current meter $\overline{u'v'}$ field is northward at all depths and both the surface altimeter value and the 1000-m current meter record show a northward eddy momentum flux of around 50 cm^2 s^{-2}. In the Agulhas Retroflection, all of the surface current records (around 200 m) show a northward flux in $\overline{u'v'}$ of around 50–200 cm^2 s^{-2} (Luyten et al. 1990), which corresponds to the large positive maximum in the mapped Geosat $\overline{u'v'}$ field in Fig. 6. So although the altimeter $\overline{u'v'}$ field may appear complex, the data are consistent with existing point measurements from long-term current arrays. Note that the magnitude of the $\overline{u'v'}$ field shows considerable scatter in the Agulhas region. This scatter is expected as the $\overline{u'v'}$ field is less spatially coherent than the velocity variance field, and the bilinear interpolation process can cross sharp gradients in the $\overline{u'v'}$ field. These sharp gradients may be small-scale features of the $\overline{u'v'}$ field, which are also apparent in the vertical current profiles, but may be augmented by the large amount of missing Geosat data in the region.

a. *Zonal average of eddy momentum flux*

One of the considerations in examining the eddy momentum flux is to determine its contribution to the zonal momentum balance in the Southern Ocean. The zonal momentum balance can be expressed in a zonally and vertically integrated form (Johnson and Bryden 1989) as

$$\int_{-H}^{0} dz \int dx \left[\frac{\partial u}{\partial t} + \frac{\partial}{\partial x}(uu) + \frac{\partial}{\partial y}(uv)\right] = \int_{-H}^{0} dz \int dx \left[fv - \frac{1}{r_0}\frac{\partial p}{\partial x} + \frac{1}{r_0}\frac{\partial \tau^x}{\partial z}\right], \qquad (5.3)$$

where u, v are the eastward and northward velocities, f is the Coriolis parameter, ρ_0 is the density of seawater, p is pressure, τ^x is the eastward stress component, and H is water depth. At the zonally unbounded latitudes of Drake Passage, the zonally and vertically integrated meridional transport must vanish so the first term on the right-hand side of Eq. (5.3) is zero. For a zonally connected ocean,

$$\int\int \frac{\partial}{\partial x}(uu)\,dx dz = 0$$

is also zero. So for steady circulation, the integrated zonal momentum balance becomes

$$\int_{-H}^{0} dz \int dx \left[\frac{\partial}{\partial y}(uv) + \frac{1}{r_0}\frac{\partial p}{\partial x}\right] = \frac{1}{r_0}\int dx\,[\tau^x_{\text{surface}} - \tau^x_{\text{bottom}}]. \qquad (5.4)$$

The right-hand side of Eq. (5.4) refers to the zonally integrated zonal wind stress minus the zonal bottom stress. Gill (1968) argued that for frictional bottom stress to directly balance the wind stress would require bottom velocities of around 20 cm s^{-1}, which are much larger than observations suggest. So bottom frictional stress alone is not sufficient to balance the wind forcing. Instead, Gill (1968) suggested that wind stress may be balanced by a divergent momentum flux out of the circumpolar region, that is, the first term on the left-hand side of the balance equation. The second term is the zonal pressure gradient acting against bottom topographic features in the circumpolar region; the balance between surface wind forcing and topographic form drag was first suggested by Munk and Palmén (1951). In the case of a flat-bottom model, such as considered by Gill, this bottom topographic form drag term is zero.

The time-averaged zonal mean horizontal momentum flux has three components:

$$\langle \overline{uv} \rangle = \langle \bar{u}\bar{v} \rangle + \langle \overline{u^*v^*} \rangle + \langle \overline{u'v'} \rangle, \qquad (5.5)$$

the zonal mean flow component $\langle \bar{u}\bar{v} \rangle$, the contribution from spatially fixed meanders about the zonal mean position of the current (the standing eddy component) $\langle \overline{u^*v^*} \rangle$, and a contribution from temporal variability (the transient eddy component) $\langle \overline{u'v'} \rangle$. The overbar refers to a time average and the $\langle\ \rangle$ brackets refer to zonal averages. Gill (1968) considered the principal part of the momentum flux was due to transient eddies and calculated that a vertically and zonally averaged net eddy momentum flux of around 100 cm^2 s^{-2} out of the circumpolar region is required to balance the momentum input by the wind.

The difficulty in testing Gill's theory is in providing zonal and vertical observations of $\overline{u'v'}$. Bryden and Heath (1985) evaluated the vertically averaged $\overline{u'v'}$ at one location southeast of New Zealand; when extrapolated around the Southern Ocean it could only balance one-quarter of the momentum input by the wind. The Geosat zonally averaged eddy momentum flux from

transient eddies is shown in Fig. 7, in comparison to the FGGE drifter results from Piola et al. (1987). Note again that the altimeter only includes geostrophic motion—the drifter results also include an ageostrophic component. In general, the magnitude of the zonally averaged surface $\langle \overline{u'v'} \rangle$ is around 5–10 cm^2 s^{-2} for both datasets, with a peak around 50°S of 27 cm^2 s^{-2} for the FGGE drifters and a statistically significant peak of 10 cm^2 s^{-2} for the Geosat data.

Following Gill (1968), the contribution of the transient eddy momentum flux to the zonal momentum balance was investigated, by comparing the momentum input by the wind over the zonally unbounded latitudes of Drake Passage from 56.5°S to 61.5°S, with the divergent eddy flux of momentum out of the band. The area integral of the zonal wind stress over this latitude band is 1.75×10^{17} dyn, derived from ECMWF wind data (Trenberth et al. 1990). The Geosat estimate of the net flux of zonally averaged $\langle \overline{u'v'} \rangle$ between the northern and southern boundaries of this circumpolar band is only -6.8 cm^2 s^{-2} and is convergent (based on zonal values significant at the 95% level). Note that this calculation is sensitive to the choice of methodology; for example, the sign can vary if one changes the significance level or includes low-reliability estimates, although the magnitude always remains small. Multiplied by the circumpolar distance at 60°S of 20 000 km, and by an average water depth of 4 km, the net flux of eddy momentum is only 5.5×10^{15} dyn into the circumpolar region. These surface flux estimates are also likely to overestimate the depth-averaged values. So the Geosat measurements indicate that the zonally averaged meridional flux of zonal momentum is at least two orders of magnitude too small to balance the momentum input by the wind, and is in fact convergent not divergent.

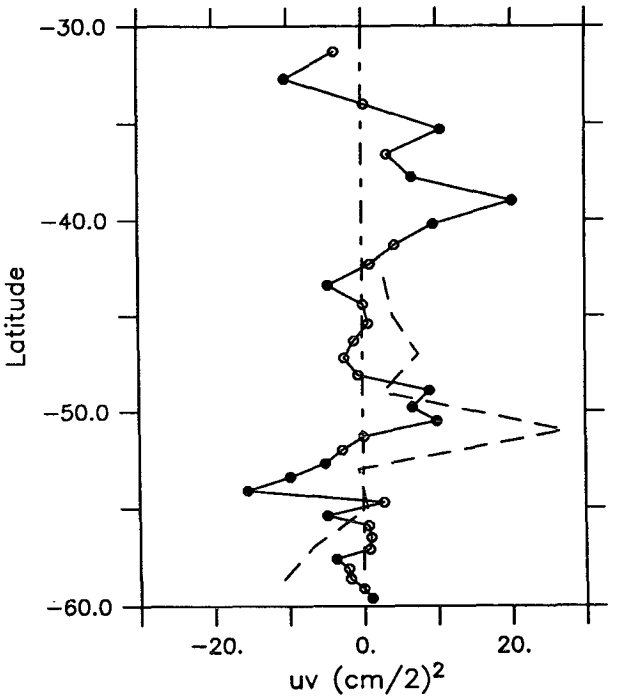

FIG. 7. Zonally averaged $\overline{u'v'}$ from Geosat crossover velocities (solid line), compared with FGGE surface drifters (Piola et al. 1987) (dashed line). Zonal values above the 95% significance level are solid filled.

b. *Streamwise averages of eddy momentum flux*

The wind forcing is predominantly zonal at the latitudes of Drake Passage, so zonal averages are useful in determining the role of horizontal eddy momentum flux in balancing the momentum input by the wind. However, it is evident from Fig. 6 that the largest $\overline{u'v'}$ values are not associated with the latitudes of maximum wind forcing around 50°S, but with the location of the mean current, especially where it interacts with topography. This suggests that the observed transient eddies may be generated by baroclinic and barotropic instabilities in the mean flow, as predicted in recent numerical models (Wolff et al. 1991; Treguier and McWilliams 1990). In this case, it is preferable to consider the transfer of momentum between the transient eddies and the mean current.

When the mean current is not strictly zonal, the meridional flux of zonal momentum ($\overline{u'v'}$) will not accurately represent the cross-stream eddy momentum flux. To rectify this problem, we have considered the divergence of eddy momentum flux in both the zonal and meridional momentum equations, respectively, which can be thought of as eddy forces, F^{eddy}, on the mean flow; that is,

$$F_x^{\text{eddy}} = -(\overline{u'u'})_x - (\overline{u'v'})_y, \tag{5.6}$$

$$F_y^{\text{eddy}} = -(\overline{u'v'})_x - (\overline{v'v'})_y, \tag{5.7}$$

where the overbar denotes time averaging, the primes denote the time-varying component, and subscripts denote spatial differentials.

We are interested in how the horizontal Reynolds stresses may transfer momentum from the eddies to the mean current; to estimate this we need to define the local direction of the mean current. The mean flow cannot be determined directly from Geosat data due to uncertainties in the marine geoid. But we get an approximate measure of the mean field from the historical dynamic topography data of Gordon and Molinelli (1982, hereafter referred to as the GM data). We use the 1° latitude by 2° longitude gridded 0/2000 dbar dynamic topography to determine the direction of the mean flow, represented by the unit vector (u_m, v_m). The horizontal Reynolds stresses ($\overline{u'u'}$, $\overline{v'v'}$, $\overline{u'v'}$) were similarly smoothed and interpolated onto a 1° latitude by 2° longitude grid, using an inverse distance weighting filter, over a 3° by 3° square centered at the crossover point. The divergence terms in

Eqs. (5.6) and (5.7) were then calculated by centered first differences at each grid point.

The contribution of the horizontal Reynolds stresses to the *alongstream* momentum balance can be found by considering the alongstream component of the eddy force on the mean flow, F_a^{eddy}; that is,

$$F_a^{\text{eddy}} = u_m F_x^{\text{eddy}} + v_m F_y^{\text{eddy}}. \qquad (5.8)$$

The mapped alongstream eddy force [Eq. (5.8)] is shown in Fig. 8a. Positive values imply that the eddy forces are imparted *to* the mean flow *by* the eddy field. Assuming these surface values are representative of the upper 1000 m, the magnitude of the depth-integrated eddy forcing on the highly energetic Agulhas Retroflection and Return Current (typically 1–8 $\text{cm}^2\ \text{s}^{-2}$) is similar to that of the local wind stress forcing. (A depth-integrated eddy force of 1 $\text{cm}^2\ \text{s}^{-2}$ is equivalent to a surface wind stress forcing of 1 dyn cm^{-2}.)

The cross-stream divergence of horizontal Reynolds stresses (i.e., the eddy forces perpendicular to the mean flow, $F_\perp^{\text{eddy}}$) can also be expressed as

$$F_\perp^{\text{eddy}} = v_m F_x^{\text{eddy}} + u_m F_y^{\text{eddy}}. \qquad (5.9)$$

Figure 8b shows a coherent alongstream pattern, which may be related to cross-stream meandering of the mean

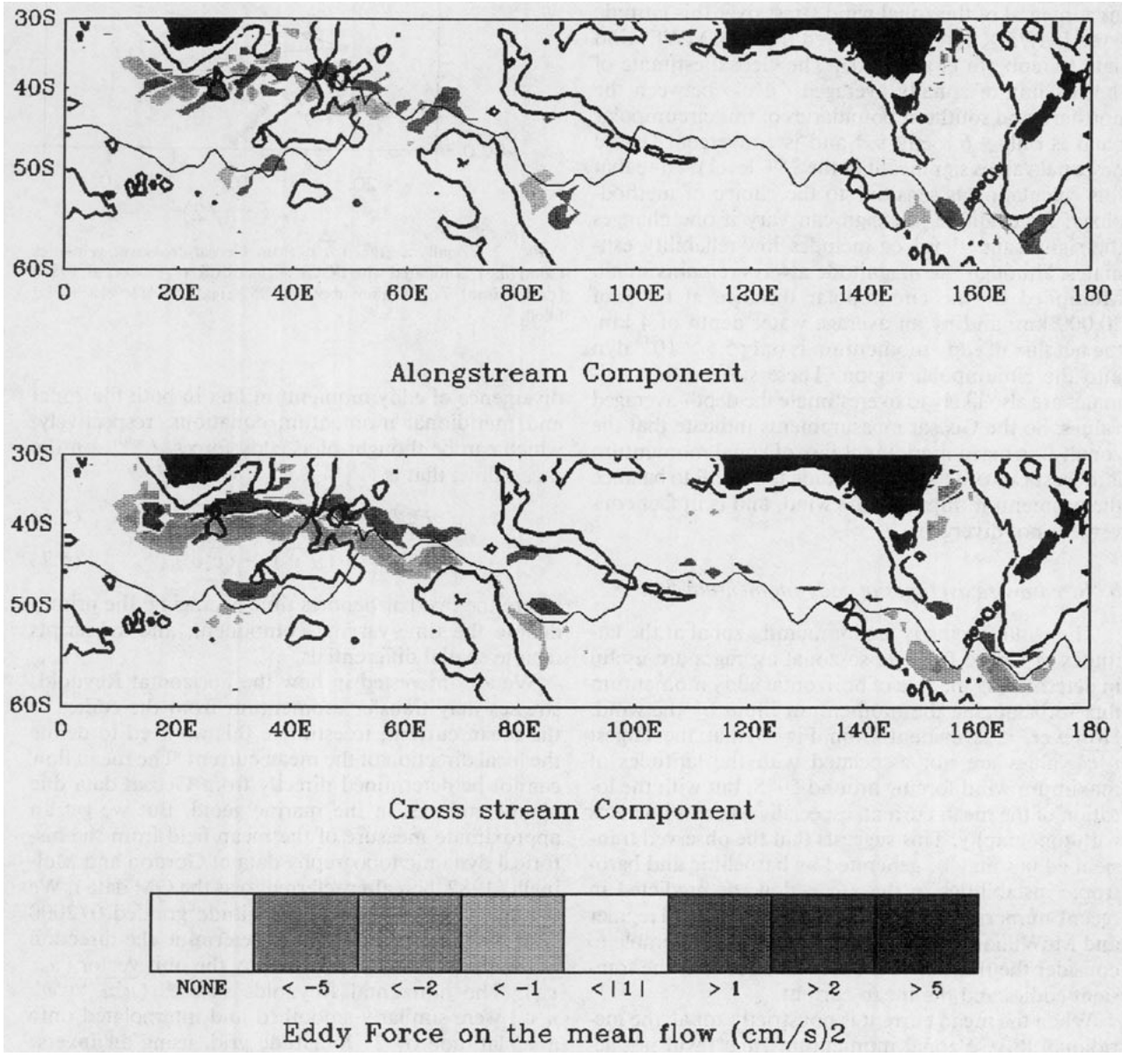

FIG. 8. (a) The magnitude of the alongstream component of the eddy force, depth averaged over the top 1000 m (in $\text{cm}^2\ \text{s}^{-2}$) [Eq. (5.8)]. (b) The magnitude of the cross-stream component from Eq. (5.9). The thin line is mean axis ACC2 (see text).

flow. The dominant term in Fig. 8b is the cross-stream gradient of the variance $(\overline{v'v'})_y$, which results from any nonstationary meanders in the mean axis of the ACC. This variance is largest at the location of the mean axis, and decreases away from the mean axis. From Eq. (5.9), this translates to positive values north of the mean current and negative to the south. The well-defined zero contour in Fig. 8b corresponds to the location of the maximum velocity variance. This provides a good altimeter-based estimate of the position of the mean axis of the ACC (Chelton et al. 1990), independent of whether the Reynolds stresses contribute to the mean alongstream velocity.

Streamwise averages of the alongstream and cross-stream eddy forces were calculated parallel to a defined mean axis of the ACC. Two definitions of the mean axis were used. The first (ACC1) is defined from the position of maximum gradient in the GM data. Use of this mean position may introduce errors in the streamwise calculation, since the highly smoothed, historical mean position could be spatially offset from the mean position over the two years of Geosat data. Moreover, in regions of sparse hydrographic data density, there may be significant errors in the position of the ACC axis from the GM data. The second mean axis (ACC2) is defined from the zero contour of Eq. (5.9) (i.e., based on the cross-stream divergence of the Geosat Reynolds stresses), which may provide a more accurate estimate of the axis of the ACC. For example, ACC2 more accurately reproduces the large meridional meanders that are known to exist at 27°E and 32°E (Lutjeharms and Ballegooyen 1988). Both mean axes are plotted in Fig. 9 for both the ACC and the Agulhas Return Current.

The streamwise average of the alongstream eddy forces for the Agulhas Return Current (20°–60°E) are shown in Fig. 10a and are multiplied by a depth of H = 1000 m as an estimate of the depth-integrated quantities. The alongstream average is similar for both definitions of the current: namely, positive 1° north of the axis (corresponding to a local convergence of momentum toward the jet) and a secondary smaller maximum 2° south of the axis. Farther north and south are negative regions, which may indicate a deceleration of the mean flow by the Reynolds stress divergence. The peak magnitude of the streamwise average, depth-integrated eddy force is almost 1 $cm^2\ s^{-2}$. Thus, in the region of the Agulhas Return Current, the present analysis indicates that the horizontal Reynolds stresses are of comparable importance to the wind stress.

For the Macquarie Ridge and the Campbell Plateau region (145°–175°E), Fig. 10b shows a broad positive band (±3°) with depth-integrated values up to 0.5 $cm^2\ s^{-2}$, and surrounding regions where the term is negative. These regions where the streamwise averages are clearly positive indicate a net convergence of horizontal Reynolds stresses, which can act to accelerate the mean flow, as predicted in recent numerical models (McWilliams et al. 1978; Wolff et al. 1991; Treguier and McWilliams 1990). For the region of the Pacific Rise, the results are sensitive to the choice of axis used. This may be because the ACC is weaker and the position of the jet axis is therefore poorly defined by the historical dataset in the region. In the ACC south of South Africa at 50°S where the jet axis is also poorly defined, the alongstream eddy force is much smaller.

For the streamwise averages along the entire circumpolar ACC path (not shown), there is a positive alongstream eddy force 2° south of the current. However, the magnitude is small; only of order 0.1 $cm^2\ s^{-2}$ for both definitions of the ACC axis. The streamwise average of the cross-stream eddy force demonstrates the same clear pattern of positive values north of the mean current and negative to the south, as noted in Fig. 8b.

6. Discussion

We have described a technique for resolving surface eddy velocity components at Geosat crossover points, with the primary aim of investigating the role of horizontal eddy momentum fluxes in the dynamical balance of the ACC. The technique provides long-term, ocean-scale measurements of surface velocity variance and horizontal eddy momentum flux in the Southern Ocean south of 30°S, with better spatial coverage than current meter moorings, and more regular sampling than can be obtained from surface drifters. Even so,

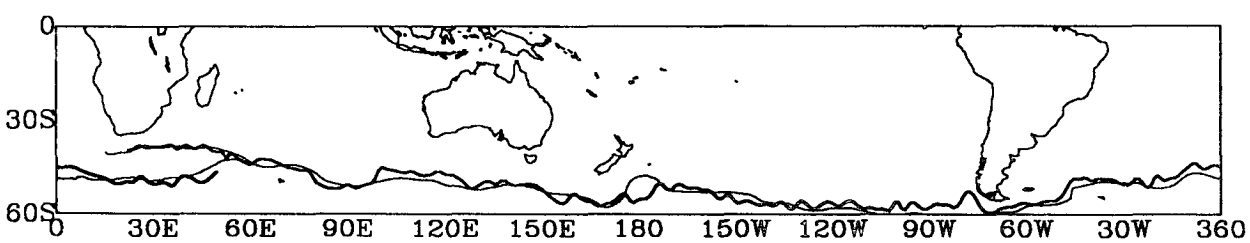

FIG. 9. Mean axis of the Antarctic Circumpolar Current, ACC1 (thin line), derived from the maximum gradient in the 0/2000 dbar dynamic topography from Gordon and Molinelli (1982). The "mean axis" is defined as the continuous circumpolar path; the Agulhas Return Current is also shown. The mean axis derived from the cross-stream divergence of eddy momentum flux, ACC2, is shown as the thick line.

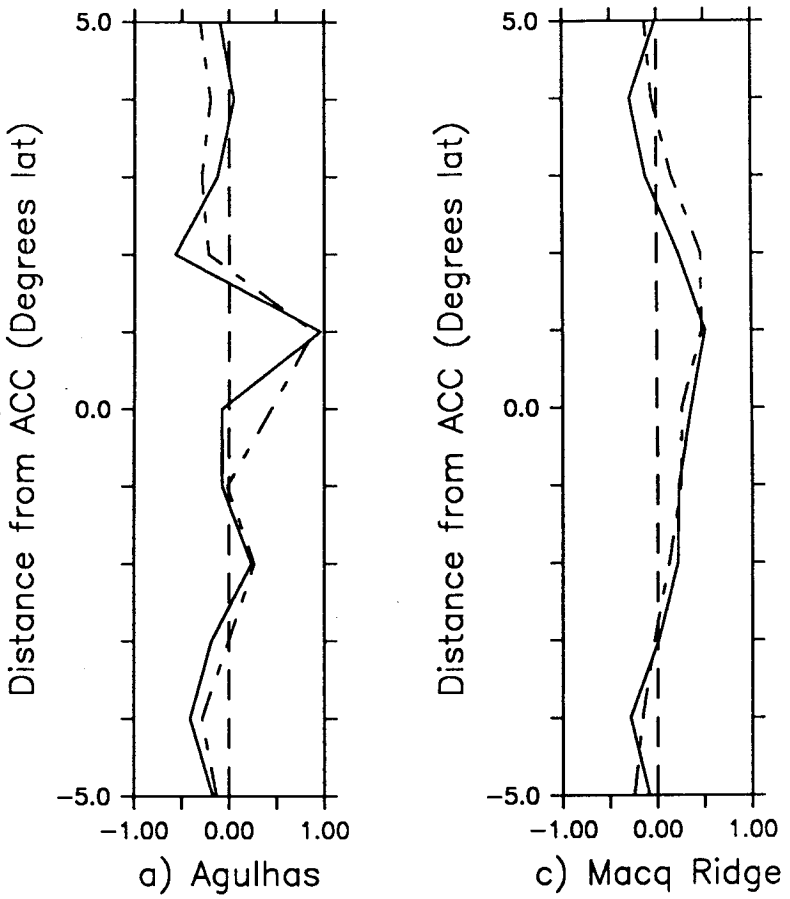

FIG. 10. Streamwise averages of the alongstream component of the eddy force, depth averaged over the top 1000 m ($cm^2 s^2$) (a) in the Agulhas Return Current (20°–60°E) and (b) for the Macquarie Ridge and Campbell Plateau region (145°–175°E). Streamwise averages are plotted as a function of the distance in degrees latitude from the chosen axis. The solid line is calculated using path ACC1; the short-long dashed line using path ACC2.

smoothing to remove the measurement noise of Geosat limits the spatial resolution of the data to around 100 km, so we may still miss a significant portion of the eddy energy at higher latitudes, where the radius of deformation decreases to around 10 km. In future work, the lower measurement noise for TOPEX/Poseidon may allow us to resolve more of the smaller-scale eddy energy in the ACC. Note that the technique resolves only the transient eddy component of variability; the time-invariant flow such as the mean current and the standing eddy component cannot be resolved from presently available altimeter data due to uncertainties in the marine geoid.

The calculated surface variability shows reasonable agreement with available in situ current records in high energy regimes: at 200 m in the Agulhas Retroflection (Luyten et al. 1990) and at 1000 m southeast of New Zealand (Bryden and Heath 1985). The magnitude and direction of the altimeter surface velocity variance is consistent with a surface amplification from the current measurements at depth. In addition, there is reasonable agreement in the time series of residual velocities from altimetry and 200-m currents in the Agulhas Retroflection from a 3-month overlapping period. Moreover, the $\overline{u'v'}$ measurements have the same sign and similar magnitude, even in the Agulhas Retroflection where there are strong spatial gradients in the eddy field. The agreement with the long-term current meter records is reassuring, as both datasets measure temporal variability at one location, with minimal spatial averaging. The measurements are made over different periods, and their consistency suggests that long-term eddy statistics may be fairly stable in the Southern Ocean, especially in regions where the mean flow and variability are constrained by topography.

The measured surface eddy variability from transient eddies was found to be distinctly anisotropic, especially in regions associated with strong mean currents or close to topographic features. The results imply that the isotropic assumption used in previous studies to calculate

EKE from alongtrack altimeter data is not valid locally, although basin-scale or zonal averages of variability are close to isotropic. Zonal averages of $\overline{v'^2}/\overline{u'^2}$ show a slight increase in the meridional component at lower latitudes. This is the opposite to basin-scale averages in the Southern Ocean from a Lagrangian analysis of surface drifters (Johnson 1989), which find the variability has a larger zonal component. The larger meridional component in the Geosat data may be influenced to some extent by measurement error, as the geometrical transformation maps more error into the north component of velocity than the east component at lower latitudes. A more significant problem is that the comparison is complicated by the different spatial and temporal scales that are included in the zonal averages. The resolution of the Geosat data is about 100 km spatially and 17 days temporally. With this resolution we may be missing a significant portion of eddy energy at higher latitudes, where the Rossby radius of deformation is small. However, the drifter data miss even more of the eddy variability because of the large space and time averaging necessary for the sparse data distribution. As noted earlier, drifters also tend to converge at fronts, biasing the sampling, and are affected to an unknown degree by windage.

The method for calculating orthogonal velocity components at altimeter crossover points is fairly sensitive to measurement error. The 4–8 cm accuracy of the Geosat data means that the measurement error can dominate the ocean signal in low energy regions. The background measurement errors, which include any errors in the geophysical corrections, have been estimated in this study (see appendix B). Only velocity variances that are above the estimated background noise are used in the analysis of horizontal eddy fluxes, either at individual crossover points or in the zonal and streamwise averages. It is expected that the TOPEX/Poseidon mission will have improved accuracy in orbits, instrument precision, and geophysical corrections. This should reduce the background measurement noise by at least a factor of 2–3 and increase the signal-to-noise ratio, thus allowing us to resolve more of the low energy regions of the ocean.

a. Zonal averages

The altimeter results show that the zonally averaged horizontal divergence of eddy momentum flux is at least an order of magnitude too small to balance the large amount of momentum input by the wind, and is also of an ambiguous sign. This result implies that other mechanisms must be more important in balancing the wind-input momentum. The main contender appears to be bottom topographic form stress, set up by eddies (Holloway 1987) or the mean flow (Munk and Palmén 1951) interacting with bottom topographic features.

Recent quasigeostrophic channel models have shown how transient and standing eddies may be important in transporting wind-input momentum vertically downward, to be balanced by bottom stress or bottom topographic form stress (Treguier and McWilliams 1990; Wolff et al. 1991). Note that the lateral boundary conditions of these channel models prohibit the meridional transport of momentum beyond the bounds of the channel walls, so the surface momentum is *forced* to be transferred vertically. The interesting result of these simple models is that an intensive eddy field develops to accommodate the large vertical momentum transfer. A simple model by Johnson and Bryden (1989) also involves the vertical transfer of zonal momentum by eddies, to be balanced by bottom form stress. This model is developed and tested for Drake Passage conditions where the lateral continental boundaries are real, and the measured horizontal eddy momentum fluxes are small [from both the current meter data (Wright 1981) and the Geosat data analyzed here]. Again the vertical eddy fluxes transfer momentum downward.

As suggested by Munk and Palmén (1951), an alternate balancing mechanism is that most of the momentum input by the wind goes directly into the surface Ekman layer, as proposed in coarse-resolution models and reinforced from the near eddy-resolving Fine Resolution Antarctic Model (FRAM) (Webb et al. 1991). The equatorward surface Ekman transport is balanced by a deep poleward return flow below the sill depth of 2000 m, which then sets up topographic form stress (P. Saunders 1992, personal communication). At 60°S, FRAM shows a northward Ekman transport of 10.5 Sv balanced by a southward return flow of 13 Sv below the sill depth of 2000 m, and finally a bottom northward flow of 2.5 Sv. The FRAM model also finds a significant eddy field in the Southern Ocean, generated by instabilities in the mean current. These eddies are coherent with depth [as found in current meter observations, e.g., Bryden and Heath (1985) and Sciremammano et al. (1980)]. There is some vertical transfer of momentum associated with these eddies, although the magnitude of these vertical eddy fluxes has not yet been determined (D. Stevens 1992, personal communication). On the basis of FRAM results, Döös and Webb (1994) argue that it is the mean meridional circulation (rather than time-variable eddies) that is responsible for much of the vertical transfer of momentum. The zonal pressure gradient associated with the deep northward geostrophic flow is of the correct sign and magnitude to yield a topographic form drag that balances the wind stress.

Whether momentum input by the wind is transferred vertically by eddy fluxes or horizontally within the mean, Ekman transport cannot be resolved using Geosat data alone. But the present results have shown conclusively that on a zonal average, the horizontal divergence of eddy momentum flux is not sufficient to balance the zonal momentum input by the wind.

b. Streamwise averages

The altimeter results clearly show that Reynolds stresses can be significant in redistributing zonal momentum laterally in the energetic regions near topographic features where Hofmann (1985) found fronts were most clearly delineated. A convergence of momentum is noted in primitive equation models with realistic topography and forcing (Semtner and Chervin 1992; D. Stevens 1992, personal communication) and has been observed in the Gulf Stream and Kuroshio Current (Schmitz 1982; Nishida and White 1982; Tai and White 1990). Quasigeostrophic numerical model results show the convergence of eddy momentum flux from transient eddies is around 0.2 to 0.5 $cm^2 s^{-2}$ for both layers (Treguier and McWilliams 1990; Wolff et al. 1991). The surface Geosat measurements (assumed representative of the top 1000 m) are of a similar magnitude in the Agulhas Return Current and near the Macquarie Ridge/Campbell Plateau. Wilkin and Morrow (1994) have compared the observed eddy-to-mean momentum flux and eddy-to-mean energy conversion with similar calculations from an eddy-resolving numerical model in the Southern Ocean region. Their comparison shows that altimeter-derived horizontal fluxes are consistent with the high-resolution model results despite the noisy Geosat data and uncertainties in the position of the mean axis of the current. Indeed, their results not only support the present results but also indicate that this technique provides a useful diagnostic tool for eddy-resolving numerical models.

While local values of the Reynolds stress divergences are large, the circumpolar streamwise averages are small. The Geosat results (assumed representative of the top 1000 m) are a factor of 2–5 smaller than the depth-averaged quasigeostrophic model results (Treguier and McWilliams 1990; Wolff et al. 1991). The differences may relate to our difficulty in defining the mean flow as some of the streamwise averages in section 5b are sensitive to the chosen definition of the mean axis. The highly smoothed mean axis based solely on the sparsely distributed GM hydrographic data (ACC1), does not include the small-scale meanders or sharper gradients evident in the fine-resolution model results. Indeed, the altimeter transient eddy component is more complex than in the model, especially around topographic features where standing eddies dominate, suggesting that small-scale meanders may contribute significantly to the observed variability. We believe the second choice of mean axis (ACC2) inferred from the more regularly sampled Geosat data, which includes more small-scale meanders, provides a more reliable mean. It also results in a positive alongstream force on the ACC by transient eddies. Resolving small spatial scales in both the mean and the variability is necessary for understanding the dynamics of eddy–mean current interactions. This is especially important in the ACC, given the combination of the depth of the ACC, the strong topographic gradients, and the decrease in the Rossby radius of deformation toward higher latitudes.

This analysis of altimeter data has demonstrated that global-coverage satellite data can be used to examine important physical processes, especially in the vast Southern Ocean where in situ observations are so sparse. The time series of orthogonal velocities at crossover points has revealed the complex structure of velocity variance and eddy momentum flux in the Southern Ocean. By including an independent measure of the mean flow, the momentum exchange between the eddies and the mean has also been estimated. The techniques developed in this study are applicable to future altimeter missions, including TOPEX/Poseidon, with the promise of improved data quality and duration.

Acknowledgments. The authors wish to acknowledge Neil White and Michael Schlax for their contributions to the Geosat datasets, and Donna Witter, who supplied the digitized version of the GM mean axis. This work was partly supported by a grant from the Australian Research Council and the Institute of Natural Resources and Environment, CSIRO Climate Change Program. RAM was supported by an Australian Post-Graduate Research Award and a CSIRO Post-Graduate Fellowship. DBC was supported by Contract 958127 from the Jet Propulsion Laboratory, funded under the TOPEX/Poseidon Announcement of Opportunity.

APPENDIX A

Accuracy of the Geometrical Transformation

a. Effect of the Coriolis parameter

The velocity components are derived assuming geostrophy. Therefore, for fixed errors in sea surface slope, the error in each velocity component, as given by Eqs. (3.4) and (3.5), is a function of f^{-1}. Because of this increase in error toward the equator, we have restricted the present analysis to latitudes south of 30°S.

b. Effect of the crossover angle

For the Geosat orbit geometry, the crossover angle decreases toward the equator and the ground tracks become more nearly parallel. Thus, we resolve the east–west component of velocity well, but the north–south component poorly. This is reflected in the error analysis: the $\cos^2\phi$ and $\sin^2\phi$ terms in (3.4) and (3.5) produce an increase in the northward error variance ($\sigma^2_{v'}$) at lower latitudes, and a decrease in the eastward error variance ($\sigma^2_{u'}$). Near 65°S, the ascending and descending ground tracks are nearly orthogonal ($\phi \sim 45°$), so the error in the sea surface slope variance $\sigma^2_{s'}$ is shared equally between the north and east velocity components.

To illustrate this problem, Fig. A1a shows the zonal average of the ratio of north and east velocity variance from the crossover velocity data as a function of latitude. A purely isotropic signal would have a $(\overline{v'^2}/\overline{u'^2})$ ratio of 1.0. Figure A1a shows that the zonally averaged velocity variance from the Geosat data is close to isotropic at 60°S, and the ratio gradually increases to have a larger meridional component at lower latitudes. This increase may be a real ocean signal but may also be influenced by the geometric transformation and the measurement error. If the SSH data were purely "noise," the $\overline{v'^2}/\overline{u'^2}$ curve would coincide with the theoretical noise curve of $(\sigma_{v'}^2/\sigma_{u'}^2) = (\cos^2\phi/\sin^2\phi)$, derived from Eqs. (3.4) and (3.5), that is, simply a function of the crossover angle. The fact that the zonally averaged $(\overline{v'^2}/\overline{u'^2})$ ratio deviates significantly from the theoretical noise curve emphasizes the high signal content of the Geosat data.

c. *Time interpolation between ascending and descending passes*

The third factor affecting the variance errors is the crossover time difference (Δt). The ascending and descending passes are not measured concurrently, but may be separated in time by up to 8.5 days for the Geosat 17-day repeat orbit. The crossover time difference varies as a function of latitude (Fig. A1b). Any change in the ocean signal or in the measurement error during the intervening time can introduce errors in the calculation of orthogonal velocity components. Thus, the $\sigma_{s'}^2$ term in Eqs. (3.4) and (3.5) may vary with the crossover time difference. This effect is apparent in Fig. A1a, where the small latitudinally periodic fluctuations in the ratio $(\overline{v'^2}/\overline{u'^2})$ are directly related to the crossover time difference (Fig. A1b). To minimize the error in $\sigma_{s'}$ we have chosen to interpolate the time series of

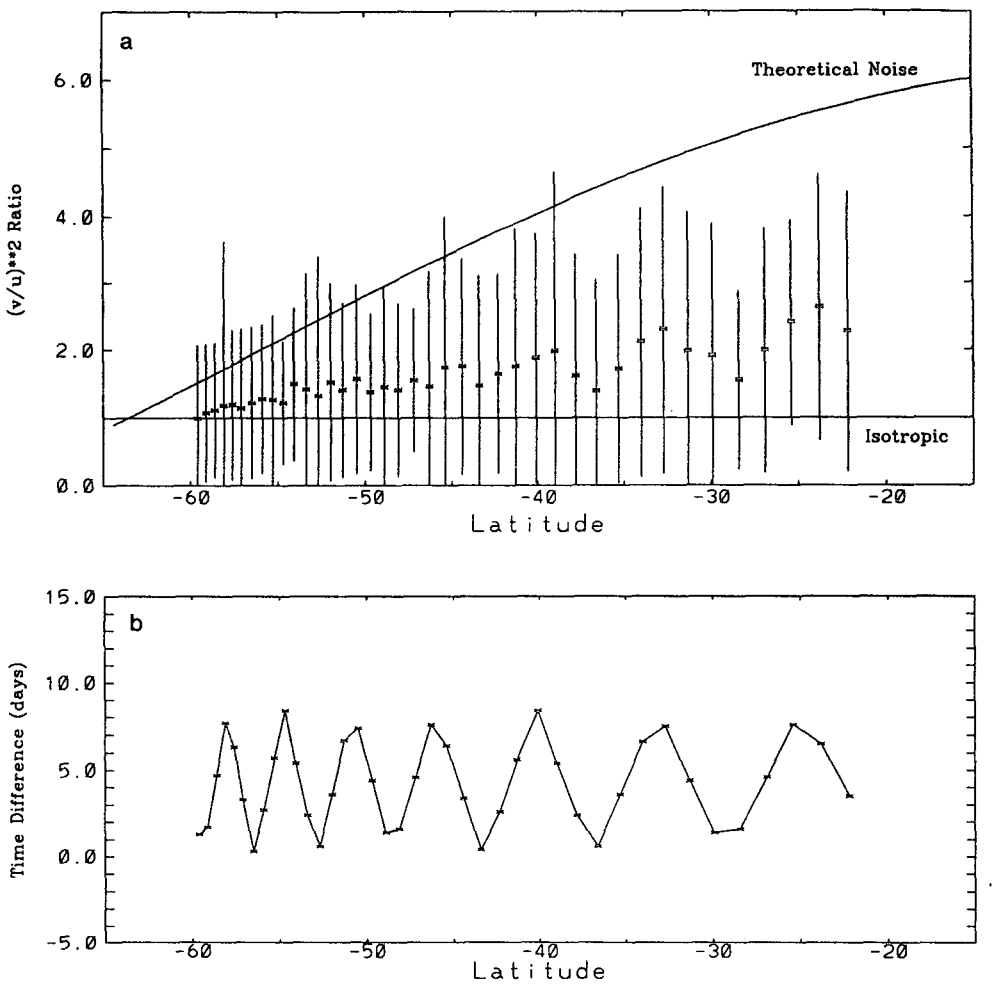

FIG. A1. (a) The zonal average of the ratio $\overline{v'^2}/\overline{u'^2}$ from velocities resolved at Geosat crossover points. The upper curve shows the theoretical error variance of σ_v^2/σ_u^2. The lower line at $\overline{v'^2}/\overline{u'^2} = 1.0$ denotes isotropic variance. The x marks the mean $(\overline{v'^2}/\overline{u'^2})$ for each crossover latitude; the vertical bars denote the standard deviation. (b) The time difference between ascending and descending passes at Geosat crossover points, which is constant along each crossover latitude.

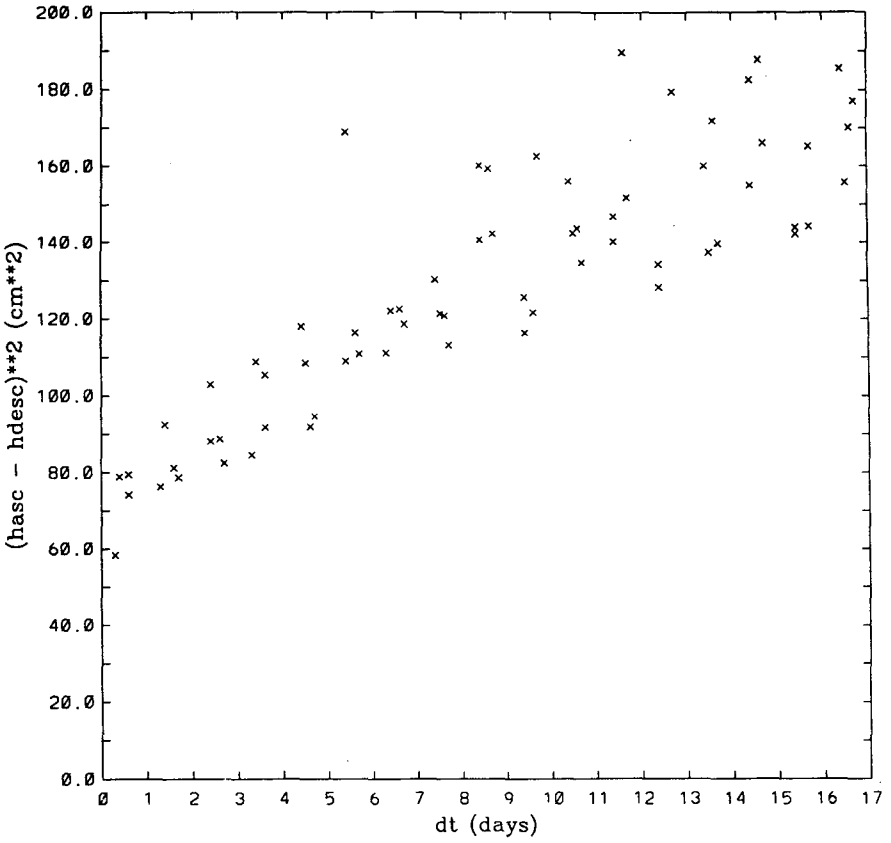

FIG. A2. Variance of the height difference $(\Delta h)^2$ between ascending and descending passes at Geosat crossover points as a function of crossover time difference (Δt).

ascending and descending velocities at each crossover point to a common 8.5-day time grid, using a natural cubic spline, before calculating orthogonal components. The interpolation procedure is applied to each ascending and descending time series at altimeter crossover points.

The interpolation to an 8.5-day time grid (rather than 17 days) increases the number of velocity estimates but does not necessarily increase the number of degrees of freedom (ndf). Current meter studies in the Southern Ocean find that the temporal scales of eddy variability are around 14 days in Drake Passage (Bryden and Pillsbury 1977) and around 20 days southeast of New Zealand (Bryden and Heath 1985). Thus, the original time series of altimeter velocities measured every 17 days gives nearly independent estimates in the Southern Ocean. The benefit of using the 8.5-day interpolation is for cases where the closest pair of ascending and descending velocities (Δt days apart) are missing, but the next closest pair (17-Δt) are available. This provides a measurement within the 17-day period, and approximately one extra degree of freedom. If both pairs are available, the 8.5-day interpolation doubles the number of samples, but still only provides one degree of freedom. This accounting is only necessary to estimate the statistical significance of the velocity variance. Note that all of the available 8.5-day interpolated velocities are used in the further analysis of velocity variance. Each crossover point will have a maximum of $N = 43$ independent velocity estimates over a two-year period, assuming there are no data gaps. On average, the ndf is around 30 because of missing data.

d. Weighting of interpolated velocities for calculating variance statistics

The interpolated velocity time series includes points that have been interpolated from their original ascending and descending measurement times by between 0.15 days and 8.35 days. Because the errors are smaller when interpolating over a small time difference, the interpolated velocities were weighted accordingly before calculating velocity variance statistics. Figure A2 shows the variance of the SSH difference between ascending and descending passes, which increases approximately linearly with crossover time difference. This increased temporal variability can be thought of as a measure of the increased error in the velocity estimation due to the crossover time difference. A weighting function was chosen based on a linear

regression of the data in Fig. A2, and gives more weight (W) to smaller crossover time differences (Δt), according to the relation

$$W = 0.646 - 0.017\Delta t. \quad \text{(A.1)}$$

The weights are only applied if we interpolate to both the ($\Delta t/2$) time and the ($8.5 - \Delta t/2$) time. If either interpolated time has missing data, the remaining point is given a weight of one.

TABLE A.1. Statistical F-test for variance. Estimates the number of degrees of freedom (ndf) required for the measured variance to be within a certain percentage (x%) of the expected variance (if there were an infinite number of measurements). For example, with 26 DF, we are within 50% of the expected variance from an infinite series.

ndf	11	26	43	157	>500	∞
Within ± x%	80%	50%	38%	20%	10%	0%

APPENDIX B

Problems Particular to the Geosat Mission

a. *Effect of missing data*

The systematic, repeated data dropouts during the Geosat mission make it sometimes difficult to distinguish noise from anomalous (but accurate) data points at undersampled crossover points. For example, one ascending or descending pass can cross an eddy or a meander of the mean current, but if the subsequent repeat passes are missing, the feature may not be sampled again. This one large velocity can then introduce a skewing of the statistics at a single crossover point that is not representative of the "undersampled" time series. With no data gaps, or a longer time series (e.g., 5 years), we would have adequate degrees of freedom so that one isolated measurement would not dominate the statistics at individual crossover points.

The ndf can be increased by spatial averaging, but we wish to preserve the smallest possible scales of variability. Alternatively, we could eliminate individual crossover points that have less than a minimum ndf. However, due to the systematic geographical patterns of missing Geosat data (Douglas and Cheney 1990), eliminating undersampled crossover points would remove important regions of high variability, especially in the boundary current regions. To resolve this problem we have chosen to edit any time series with less than 26 df, and remove outlying velocities. The cutoff at 26 df was chosen from the standard F-test table (Table A.1), as the level at which the measured variance should be within 50% of the expected variance from an infinite time series.

The editing procedure is as follows. First, the statistical sample size for the estimate of the standard deviation was increased by ensemble averaging over all of the ($V_{a'}$, $V_{d'}$) velocity measurements over three zonally adjacent crossover points. This combines data with the same crossover time differences and is more likely to average over homogeneous oceanic conditions, since ocean variability tends to be more coherent zonally than meridionally in the Southern Ocean. Individual ($V_{a'}$, $V_{d'}$) velocities at the central crossover point are then tested, and any velocities larger than $n = 2.5$ times the standard deviation are rejected. Different values of n have varying effects of the EKE, the $\overline{v'^2}/\overline{u'^2}$ ratio, and the total number of rejected data points. The 2.5 standard deviation level was chosen as a trade-off between reducing the northward error in the velocity variance due to anomalous points and maintaining the original variance and number of data points.

Imposing the 2.5 standard deviation editing criteria removes less than 3% of the data but reduces the total velocity variance by 12%. It also reduces the overall average $\overline{v'^2}/\overline{u'^2}$ ratio from 1.5 to 1.34, indicating that the top 3% of the outliers have a larger v' component, consistent with "noisy" or anomalous data. The 2.5 standard deviation edit has little effect on the zonal average of the ($\overline{v'^2}/\overline{u'^2}$) ratio at high latitudes, but substantially reduces the ($\overline{v'^2}/\overline{u'^2}$) ratio at lower latitudes, especially when the crossover time difference is large. For example at 33°S, the zonal average of ($\overline{v'^2}/\overline{u'^2}$) is 2.6 with no editing of outliers, compared to 1.9 with the 2.5 standard deviation edit. Removing these velocities has a significant effect on the EKE, and the rejected data could be real, but undersampled variability. Thus the 2.5 standard deviation edit is not an ideal method, but has been adopted here to cope with the frequent data dropouts and the short (2 year) record length of the Geosat time series. Altimetric missions such as TOPEX/Poseidon will have higher accuracy, fewer data dropouts, and a longer record, so that this editing criteria should not be necessary.

b. *Effect of the background noise in low energy regions*

The discussion of errors in this section has concentrated on all of the crossover data, irrespective of whether the measurements are in high or low energy regions. However, spectral analysis of Geosat along-track residual SSHs has demonstrated that the background measurement error can dominate the ocean signal in low eddy energy regions (Le Traon et al. 1990; Stammer and Boning 1992; Morrow 1992). The low eddy energy can occur in isolated pockets, and also over vast regions such as the eastern Pacific, from 180°E to 80°W, and 30° to 50°S (Zlotnicki et al. 1989; Chelton et al. 1990). The combination of low energy and low latitudes is particularly troublesome, as the geometrical transformation will tend to map the dominant measurement error into the northward velocity component [see Eqs. (3.4) and (3.5)]. Thus, it is im-

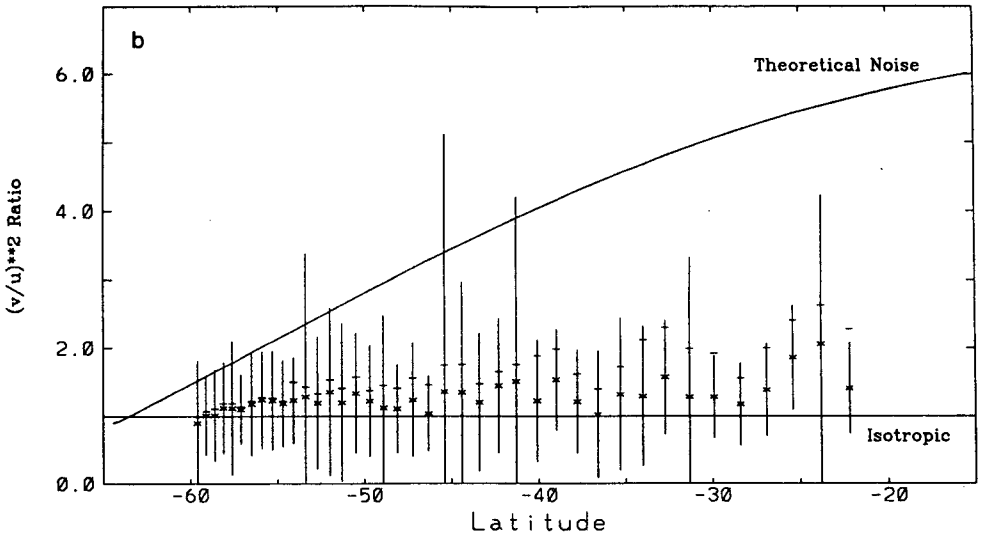

FIG. B1. As in Fig. A1a but for velocity variances above the estimated background noise level.

portant to estimate whether the measured velocities are above the background noise level.

The background noise in the residual height field is estimated by a regression fit through the data in Fig. A2. The simple regression gives a variance of the residual height difference, $\sigma^2_{\Delta h}$, that increases linearly with crossover time difference, Δt; that is,

$$\sigma^2_{\Delta h} = 64. + 6.7\Delta t. \qquad \text{(B.1)}$$

The variance of the residual height difference at zero time lag is around 64 cm^2, giving an rms error at zero lag of around 8 cm. This 8 cm error will include residual orbit error and long wavelength measurement errors (e.g., wet troposphere correction, sea-state bias effects, etc.). The estimated background height variance in Eq. (B.1) has a constant value at each crossover latitude since Δt depends only on latitude (see Fig. A1b). This value is propagated through the velocity calculations at each crossover latitude in order to estimate the error variances in the geostrophic velocities and in the orthogonal north/east components.

The zonal averages of the $(\overline{v'^2}/\overline{u'^2})$ ratio were then recalculated, using only the orthogonal velocity variances that are above the maximum estimated background noise [derived from Eq. (A.2)], and including the 2.5 standard deviation edit. The results in Fig. B1 show the zonal averages are substantially reduced and almost isotropic at low latitudes. For example, at 33°S the zonal average of the ratio of $(\overline{v'^2}/\overline{u'^2})$ has been reduced by a factor of 2 from the original unedited data. This result gives some confidence that in regions where the signal-to-noise ratio is greater than one, the orthogonal transformation method is providing reliable results.

REFERENCES

Bryden, H. L., 1979: Poleward heat flux and conversion of available potential energy in Drake Passage. *J. Mar. Res.*, **37**, 1–22.

——, and R. D. Pillsbury, 1977: Variability of deep flow in the Drake Passage from year-long current measurements. *J. Phys. Oceanogr.*, **7**, 803–810.

——, and R. A. Heath, 1985: Energetic eddies at the northern edge of the Antarctic Circumpolar Current in the South West Pacific. *Progress in Oceanography*, Vol. 14, Pergamon, 65–87.

Chelton, D. B., 1988: WOCE/NASA Altimeter Algorithm Workshop, Tech. Rep. 2, U.S. Planning Office for World Ocean Circulation Experiments, Texas A&M University, College Station, TX, 70 pp.

——, and M. G. Schlax, 1993: Spectral characteristics of time-dependent orbit errors in altimeter height measurements. *J. Geophys. Res.*, in press.

——, M. G. Schlax, D. L. Witter, and J. G. Richman, 1990: Geosat altimeter observations of the surface circulation of the Southern Ocean. *J. Geophys. Res.*, **95**(C10), 17 877–17 904.

Cheney, R. E., J. G. Marsh, and B. D. Beckley, 1983: Global mesoscale variability from colinear tracks of Seasat altimeter data. *J. Geophys. Res.*, **88**(C7), 4343–4354.

——, B. C. Douglas, R. W. Agreen, L. Miller, D. L. Porter, and N. S. Doyle, 1987: Geosat altimeter geophysical data records user handbook. NOAA Tech. Memo. NOS NGS-46, 30 pp.

Daniault, N., and Y. Menard, 1985: Eddy kinetic energy distribution in the Southern Ocean from altimetry and FGGE drifting buoys. *J. Geophys. Res.*, **90**(C6), 11 877–11 889.

deSzoeke, R. A., and M. D. Levine, 1981: The advective flux of heat by mean geostrophic motions in the Southern Ocean. *Deep-Sea Res.*, **28**(10), 1057–1085.

Döös, K., and D. J. Webb, 1994: The Deacon cell and the other meridional cells of the Southern Ocean. *J. Phys. Oceanogr.*, **24**, 429–442.

Douglas, B. C., and R. E. Cheney, 1990: Geosat: Beginning a new era in satellite oceanography. *J. Geophys. Res.*, **95**(C3), 2833–2836.

Fu, L.-L., and V. Zlotnicki, 1989: Observing oceanic mesoscale eddies from Geosat altimetry: Preliminary results. *Geophys. Res. Lett.*, **16**(5), 457–460.

Gill, A. E., 1968: A linear model of the Antarctic Circumpolar Current. *J. Fluid Mech.*, **32**, 465–488.

Gordon, A. L., 1981: Seasonality of Southern Ocean sea ice. *J. Geophys. Res.*, **86**, 4193–4197.

——, and H. W. Taylor, 1975: Heat and salt balance within the cold waters of the World Ocean. *Numerical Models of Ocean Circulation*, National Academy of Science, 54–56.

——, and E. Molinelli, 1982: *Southern Ocean Atlas.* Columbia University Press, 200 pp.

Haines, B. J., G. H. Born, G. W. Rosborough, J. G. Marsh, and R. G. Williamson, 1990: Precise orbit computation for the Geosat Exact Repeat Mission. *J. Geophys. Res.*, **95**(C3), 2871–2885.

Hofmann, E. E., 1985: The large-scale horizontal structure of the Antarctic Circumpolar Current from FGGE drifters. *J. Geophys. Res.*, **90**(C4), 7087–7097.

Holloway, G., 1987: Systematic forcing of large-scale geophysical flows by eddy–topography interaction. *J. Fluid Mech.*, **184**, 463–476.

Hulbert, H. E., 1986: Dynamic transfer of simulated altimeter data into subsurface information by a numerical ocean model. *J. Geophys. Res.*, **91**(C2), 2372–2400.

Johnson, G. C., and H. L. Bryden, 1989: On the size of the Antarctic Circumpolar Current. *Deep-Sea Res.*, **36**, 39–53.

Johnson, M. A., 1989: Southern Ocean surface characteristics from FGGE buoys. *J. Phys. Oceanogr.*, **19**, 696–705.

Large, W. G., and H. van Loon, 1989: Large scale, low frequency variability of the 1979 FGGE surface buoy drifts and winds over the Southern Hemisphere. *J. Phys. Oceanogr.*, **19**, 696–705.

Le Traon, P.-Y., M.-C. Rouquet, and C. Boissier, 1990: Spatial scales of mesoscale variability in the north east Atlantic as deduced from Geosat data. *J. Geophys. Res.*, **95**(C11), 20 267–20 285.

Lutjeharms, J. R. E., and R. C. van Ballegooyen, 1988: The retroflection of the Agulhas Current. *J. Phys. Oceanogr.*, **18**, 1570–1583.

Luyten, J., A. Spencer, S. Tarbell, K. Luetkemeyer, P. Flament, J. Toole, M. Francis, and S. Bennett, 1990: Moored current meter, AVHRR, CTD and drifter data from the Agulhas Current and Retroflection region (1985–1987). Volume XLII. Woods Hole Oceanographic Institute Tech. Rep. WHOI-90-30.

Marshall, J., D. Olbers, H. Ross, and D. Wolf-Gladrow, 1993: Potential vorticity constraints on the dynamics and hydrography of the Southern Ocean. *J. Phys. Oceanogr.*, **23**, 465–487.

McCartney, M. S., 1976: The interaction of zonal currents with topography with applications to the Southern Ocean. *Deep-Sea Res.*, **23**, 413–427.

McWilliams, J. C., and H. S. Chow, 1981: Equilibrium geostrophic turbulence I: A reference solution in a beta plane channel. *J. Phys. Oceanogr.*, **11**, 921–949.

——, W. R. Holland, and H. S. Chow, 1978: A description of numerical Antarctic Circumpolar Currents. *Dyn. Atmos. Oceans*, **2**, 213–291.

Morrow, R. A., 1992: Surface eddy variability and eddy momentum flux in the Southern Ocean from Geosat altimetry. Ph.D. thesis, University of Sydney.

——, J. A. Church, R. Coleman, D. B. Chelton, and N. White, 1992: Eddy momentum flux and its contribution to the Southern Ocean momentum balance. *Nature*, **357**, 482–484.

Munk, W. H., and E. Palmén, 1951: Note on the dynamics of the Antarctic Circumpolar Current. *Tellus*, **3**, 53–55.

Nishida, H., and W. B. White, 1982: Horizontal eddy fluxes of momentum and kinetic energy in the near-surface of the Kuroshio Extension. *J. Phys. Oceanogr.*, **12**, 160–170.

Parke, M. E., R. L. Stewart, D. L. Farless, and D. E. Cartwright, 1987: On the choice of orbits for an altimetric satellite to study ocean circulation and tides. *J. Geophys. Res.*, **92**(C11), 11 693–11 707.

Patterson, S. L., 1985: Surface circulation and kinetic energy distributions in the Southern Hemisphere oceans from FGGE drifting buoys. *J. Phys. Oceanogr.*, **15**, 865–884.

Piola, A. R., H. A. Figueroa, and A. A. Bianchi, 1987: Some aspects of the surface circulation south of 20°S revealed by First GARP Global Experiment drifters. *J. Geophys. Res.*, **92**(C5), 5101–5114.

Preisendorfer, R. W., 1988: *Principal Component Analysis in Meteorology and Oceanography.* Elsevier, 425 pp.

Richardson, P. L., 1983: Eddy kinetic energy in the North Atlantic from surface drifters. *J. Geophys. Res.*, **88**(C7), 4355–4367.

Sandwell, D. T., and B. Zhang, 1989: Global mesoscale variability from the Geosat Exact Repeat Mission: Correlation with depth. *J. Geophys. Res.*, **94**(C12), 17 971–17 984.

Schlax, M. G., and D. B. Chelton, 1992: Frequency domain diagnostics for linear smoothers. *J. Amer. Statist. Assoc.*, **87**, 1070–1081.

Schmitz, W. J., 1982: A comparison of the mid-latitude eddy fields in the western North Atlantic and the North Pacific Oceans. *J. Phys. Oceanogr.*, **12**, 208–210.

Sciremammano, F., Jr., R. D. Pillsbury, W. D. Nowlin, and T. Whitworth, 1980: Spatial scales of temperature and flow in Drake Passage. *J. Geophys. Res.*, **85**(C7), 4015–4028.

Semtner, A. J., and R. M. Chervin, 1992: Ocean general circulation from a global eddy-resolving model. *J. Geophys. Res.*, **97**(C4), 5493–5550.

Stammer, D., and C. W. Boning, 1992: Mesoscale variability in the Atlantic Ocean from Geosat altimetry and WOCE high-resolution numerical modeling. *J. Phys. Oceanogr.*, **22**, 732–752.

Tai, C.-K., and W. B. White, 1990: Eddy variability in the Kuroshio Extension as revealed by Geosat altimetry: Energy propagation away from the jet, Reynolds stress and seasonal cycle. *J. Phys. Oceanogr.*, **20**, 1761–1777.

Thompson, S. R., 1993: Estimation of the transport of heat in the Southern Ocean using a fine resolution numerical model. *J. Phys. Oceanogr.*, **23**, 2493–2497.

Treguier, A. M., and J. C. McWilliams, 1990: Topographic influences on wind-driven, stratified flow in a β-plane channel: An idealized model of the Antarctic Circumpolar Current. *J. Phys. Oceanogr.*, **20**, 321–343.

Trenberth, K. E., W. G. Large, and J. G. Olson, 1990: The mean annual cycle in global ocean wind stress. *J. Phys. Oceanogr.*, **20**, 1742–1760.

van Gysen, H., R. Coleman, R. Morrow, B. Hirsch, and C. Rizos, 1992: Analysis of collinear passes of satellite altimeter data. *J. Geophys. Res.*, **97**(C2), 2265–2277.

Webb, D. J., P. D. Killworth, A. C. Coward, and S. R. Thompson, 1991: *The FRAM Atlas of the Southern Ocean.* Natural Environment Research Council.

Wilkin, J., and R. A. Morrow, 1994: Eddy kinetic energy and momentum flux in the Southern Ocean: Comparison of a global eddy-resolving model with altimeter, drifter and current-meter data. *J. Geophys. Res.*, **99**(C4), 7903–7916.

Witter, D. L., and D. B. Chelton, 1991: An apparent wave-height dependence in the sea-state bias in Geosat altimeter range measurements. *J. Geophys. Res.*, **96**, 8861–8867.

Wolff, J.-O., E. Maier-Reimer, and D. L. Olbers, 1991: Wind-driven flow over topography in a zonal β-plane channel: A quasi-geostrophic model of the Antarctic Circumpolar Current. *J. Phys. Oceanogr.*, **21**, 236–264.

Wright, D. G., 1981: Baroclinic instability in Drake Passage. *J. Phys. Oceanogr.*, **11**, 231–246.

Zlotnicki, V., L.-L. Fu, and W. Patzert, 1989: Seasonal variability in global sea level observed with Geosat altimetry. *J. Geophys. Res.*, **94**(C12), 17 959–17 969.

——, A. Hayashi, and L.-L. Fu, 1990: The JPL-Oceans 8902 version of the Geosat altimetry data. Jet Propulsion Laboratory Tech. Rep. JPL D-6939.